Skull Morphology of the Lizard *Ptychoglossus vallensis* (Squamata: Alopoglossidae) With Comments on the Variation Within Gymnophthalmoidea

CRISTIAN HERNÁNDEZ MORALES,[1,2,3*] PEDRO L. V. PELOSO,[3,4] WILMAR BOLÍVAR GARCÍA,[1] AND JUAN D. DAZA[5]

[1]Departamento de Biología, and Grupo de Investigación en Ecología Animal, Universidad del Valle, Cali, Valle del Cauca, Colombia

[2]Intituto de Ciências Biologicas, Programa de Pós-Graduação em Zoologia, Museu Paraense Emílio Goeldi/Universidade Federal do Pará, Belém, Pará, Brazil 66040-170

[3]Museu Paraense Emílio Goeldi, Coordenação de Zoologia, Belém, Pará, Brazil

[4]Division of Invertebrate Zoology, American Museum of Natural History, New York, New York 10024

[5]Department of Biological Sciences, Sam Houston State University, Huntsville, Texas 77341

ABSTRACT

In recent years, major changes have been proposed for the phylogenetic relationships within the Gymnophthalmoidea, including the description of Alopoglossidae. Recent studies relied primarily on molecular data and have not accounted for evidence from alternative sources, such as morphology. In this study, we provide a detailed bone-by-bone description of the skull of *Ptychoglossus vallensis* and compare this species with other gymnophthalmoideans. The description was based on 10 cleared-and-stained specimens, four disarticulated skulls, and computed microtomography data of *P. vallensis*. Most recent phylogenetic hypothesis for the Gymnophthalmoidea was used as a framework to compare the skull of *P. vallensis* with other species of the Alopoglossidae, Gymnophthalmidae, and Teiidae. Marked similarities between alopoglossids and gymnophthalmids were observed in contrast to teiids, probably due to convergence generated by miniaturization. We also qualitatively analyzed the kinesis of the skull of *P. vallensis* concluding that is highly akinetic, a trait commonly evolved in fossorial, primarily burrowing squamates. We also describe one unique osteological feature for Alopoglossidae that is not known in any other squamate group. Anat Rec, 302:1074–1092, 2019. © 2018 Wiley Periodicals, Inc.

Key words: kinesis; Lacertoidea; miniaturization; skull morphology; Teiidae

Additional Supporting Information may be found in the online version of this article.

Grant sponsor: Conselho Nacional de Desenvolvimento Científico e Tecnológico; Grant numbers: 313680/2014-0, 400252/2014-7, 400252/2014-7 7, 313680/2014-0; Grant sponsor: Department of Biological Sciences at Sam Houston State University; Grant sponsor: National Science Foundation; Grant number: DEB 1657648; Grant sponsor: Coordenação de Aperfeiçoamento de Pessoal de Nível Superior.

*Correspondence to: Cristian Hernández Morales. Fax: +55 91 3075 6272. E-mail: nandezsendo@gmail.com

Received 23 January 2018; Revised 21 August 2018; Accepted 18 September 2018.

DOI: 10.1002/ar.24038

Published online 24 November 2018 in Wiley Online Library (wileyonlinelibrary.com).

The Alopoglossidae is a recently described family of neotropical lizards that comprises two genera, *Alopoglossus* (with 9 valid nominal species) and *Ptychoglossus* (15 valid nominal species). This family is distributed from Costa Rica, through northern South America, both east and west of the Andes, and across the Amazon (Harris, 1994; Köhler et al., 2012; Uetz et al., 2018). The Alopoglossidae was described by Goicoechea et al. (2016), based on the interpretation of phylogenetic analyses, to include all members of the former Gymnophthalmidae subfamily Alopoglossinae, using concatenated datasets of sequences from 48 genes. The authors implemented several tree-search strategies, with variable results among them. The topology based on direct optimization parsimony recovered the Alopoglossidae as the sister group of the Teiidae + Gymnophthalmidae (Fig. 1), thus rendering the Gymnophthalmidae polyphyletic. This new analysis contrasts with the most traditional and widely adopted taxonomic arrangement, in which the Alopoglossidae is the basal most gymnophthalmid subfamily (Pellegrino et al., 2001; Castoe et al., 2004; Peloso et al., 2011; Pyron et al., 2013; Goicoechea et al., 2016 [maximum likelihood analysis]). In this article, we follow the taxonomic arrangement of Goicoechea et al. (2016).

Most recent discussion about the evolution of the Gymnophthalmoidea has focused on molecular data, whereas the morphological variation of this phenotypically diverse and complex group has remained ignored. The lack of attention to phenotypic characters resulted in problems, including vague and confusing morphological diagnosis of the subgroups within the Gymnophthalmoidea. For example, the Gymnophthalmidae (*sensu* Presch, 1983) is diagnosed by only a few morphological characters observed in a few taxa (Presch, 1980; Estes et al., 1988; Hoyos, 1998; Conrad, 2008; Evans, 2008; Gauthier et al., 2012). Previous synapomorphies of the family Gymnophthalmidae *s.l.* are not present in all members, and the majority of the putative synapomorphies for clades within the family seem to be influenced by homoplasy (Doan and Castoe, 2005). This problem is also aggravated by the scattered and only partially studied morphological details for most taxa (e.g., Bell et al., 2003; Evans, 2008; Guerra and Montero, 2009). There are only three references to skull morphology of the Alopoglossidae. MacLean (1974) provided the earliest known description of the osteology of one taxon in this group, with some general comments and illustrations of the skull of *Alopoglossus buckleyi*. Presch (1980) illustrated the palate, the supratemporal region, and the hyoid apparatus of *Ptychoglossus festae*. The ontogenetic development of the skull of *Ptychoglossus bicolor* was described in detail, with emphasis on the chondrocranial elements, by Hernández-Jaimes et al. (2012).

Current hypothesis of relationships within the Gymnophthalmoidea (Goicoechea et al., 2016) provides a great opportunity for reconsideration of the morphological evolution in the group, particularly within the Alopoglossidae. Herein, we provide a comparative analysis of the structure of the skull in *Ptychoglossus vallensis* Harris, 1994 and contrast this species with other gymnophthalmids, teiids, and alopoglossids. Our main goals are to: (1) provide a thorough description of the skull of *P. vallensis* and (2) provide a *better* understanding of the morphology of this poorly studied lizard taxon, including putative synapomorphies for this new lizard family.

MATERIAL AND METHODS

Fourteen specimens of *P. vallensis* (Supplementary Material) were collected in localities throughout Southwestern Colombia (Departamentos Valle del Cauca and Cauca). This species dwells in dry tropical forests and was sampled with a collecting permit issued by the Autoridad Nacional de Licencias Ambientales (ANLA, http://www.anla.gov.co; wildlife collecting permit, resolution 1070h of 28 August 2015). Soon after capture, the specimens were euthanized with 0.1 mL intracoelomic injection of lidocaine (3%) using a mini-syringe in the abdominal area (Leary et al., 2013). We measured the snout-to-vent length (SVL) and determined the sex of adult specimens by the presence or absence of hemipenes. We classified specimens as adults or subadults based on the postnatal ossification sequence (Maisano, 2001).

Specimens destined for clearing and double staining (Maisano, 2008) were preserved with 10% neutral buffered formalin solution, then transferred to 70% ethanol solution. From the original series of 14 specimens, 10 were cleared and stained and 4 specimens were disarticulated using bacterial maceration (Hildebrand, 1968). To obtain disarticulated skull bones, we removed the head of specimens immediately after euthanizing them and the rest of the body was fixed in formalin. Heads were placed directly in tap water for several days in an open container at room temperature (~24°C). Bones were recovered by filtering the solution with a black mesh. To stop bacterial decay, specimens were rinsed and placed in 70% ethanol for 24 hr. Bones were dried at room temperature and stored in labeled plastic containers.

We also obtained a high-resolution computed microtomography (μCT) scan of specimens of *Alopoglossus buckleyi* (AMNH113762), *Loxopholis guianense* (YPM HERR.015357), *Ptychoglossus plicatus* (AMNH114307), and *P. vallensis* (AMNH 119239 in a GE Pheonix Vtome Xs Micro Computed Tomography at the Microscopy and Image Facility at the American Museum of Natural History (MIF-AMNH). The specimens were scanned with variable resolutions, ranging from 15 to 60 μm with x-ray operating at 100–200 kV and 80–160 mA. Three-dimensional μCT data reconstructions and 3D image visualizations were generated in VGStudio MAX version 2.2 (Volume Graphics, Heidelberg, Germany). TIFF images and 3D models are available in morphosource (http://www.morphosource.org/Detail/ProjectDetail/Show/project_id/600).

For comparisons, we cleared and stained additional gymnophthalmoid specimens: Alopoglossidae: *Alopoglossus angulatus*, *Alopoglossus altiventris*, *Ptychoglossus stenolepis*; Gymnophthalmidae: *Echinosaura palmeri*, *Pholidobolus vertebralis*, *Potamites ecpleopus*, *Riama laevis*, *Riama estriata*, and *Cercosaura ocellata*. We also analyzed dry skulls of the teiid species *Ameiva ameiva*, *Cnemidophorus lemniscatus*, *Crocodilurus amazonicus*, *Drecaena guianensis*, *Kentropyx calcarata*, *Salvator duseni*, and *Tupinambis teguixin*. A complete list of examined specimens is given in Supplementary Material.

Anatomical observations were made under a Leica EZ4 dissecting microscope (Leica Macrosystems, Wetzlar, Germany). Photographs were taken with a Nikon DS-Ril digital camera attached to a Nikon SMZ-1500 stereoscopic microscope (Nikon Instruments, Tokyo, Japan) at the Image Facility at the Universidad del Valle (Colombia).

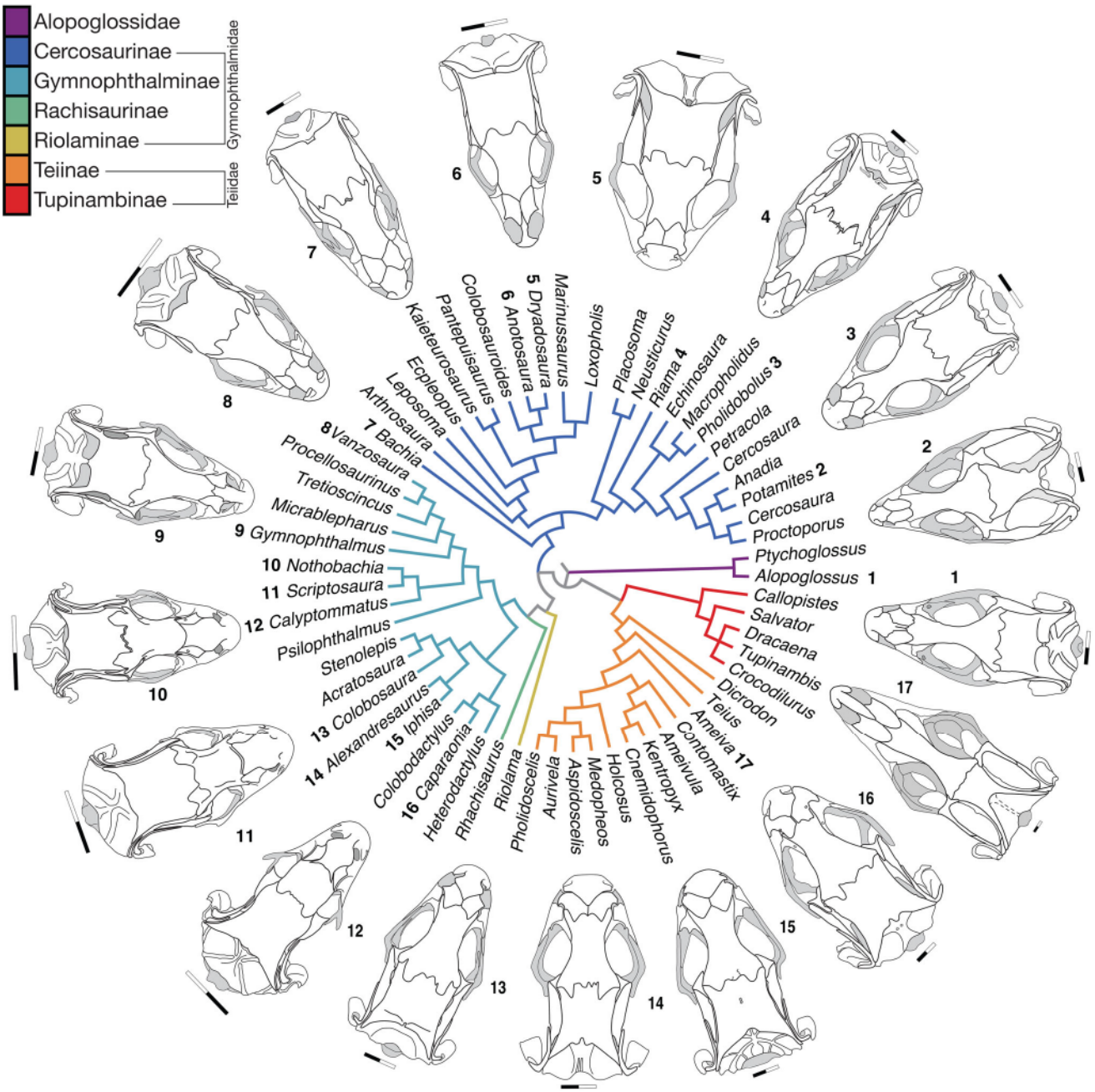

Fig. 1. Relationships among the Gymnophthalmoidea genera with morphological variation of the skull morphology in Teioidea. (1) *Alopoglossus buckleyi*, (2) *Potamites ecpleopus*, (3) *Pholidobolus vertebralis*, (4) *Riama unicolor*, (5) *Dryadosaura nordestina*, (6) *Anotosaura vanzolinia*, (7) *Bachia bresslaui*, (8) *Vanzosaura rubricuda*, (9) *Gymnophthalmus especiosus*, (10) *Nothobachia ablephara*, (11) *Scriptosaura catimbau*, (12) *Calyptommatus nicterus*, (13) *Colobosaura modesta*, (14) *Alexandresaurus camacan*, (15) *Iphisa elegans*, (16) *Caparaonia itaiquara*, and (17) *Ameiva ameiva*. Scale bar = 2 mm.

Focus staking was done using the NIS-Elements BR, using between three and five pictures per bone. Drawings were rendered using CorelDRAW(R) Technical Suite X6 over digital photographs, following recommendations in Daza et al. (2008) to improve accuracy. Anatomical terminology follows previous lizard descriptions, detailed in Oelrich (1956), Jollie (1960), Bell et al. (2003), and Evans (2008).

RESULTS

General Morphology of the Articulated Skull

The skull of *P. vallensis* (Fig. 2) is miniaturized ($\bar{x}$ = 10.8 mm, N = 2; CD-UV 3077, 2143). The orbits are large, and the rostrum is broad and rounded. The external nares are rounded and oriented laterally (Fig. 2C,H). The lacrimal is absent. The postorbital and supratemporal bars are complete (Fig. 2C,H). There is a single element

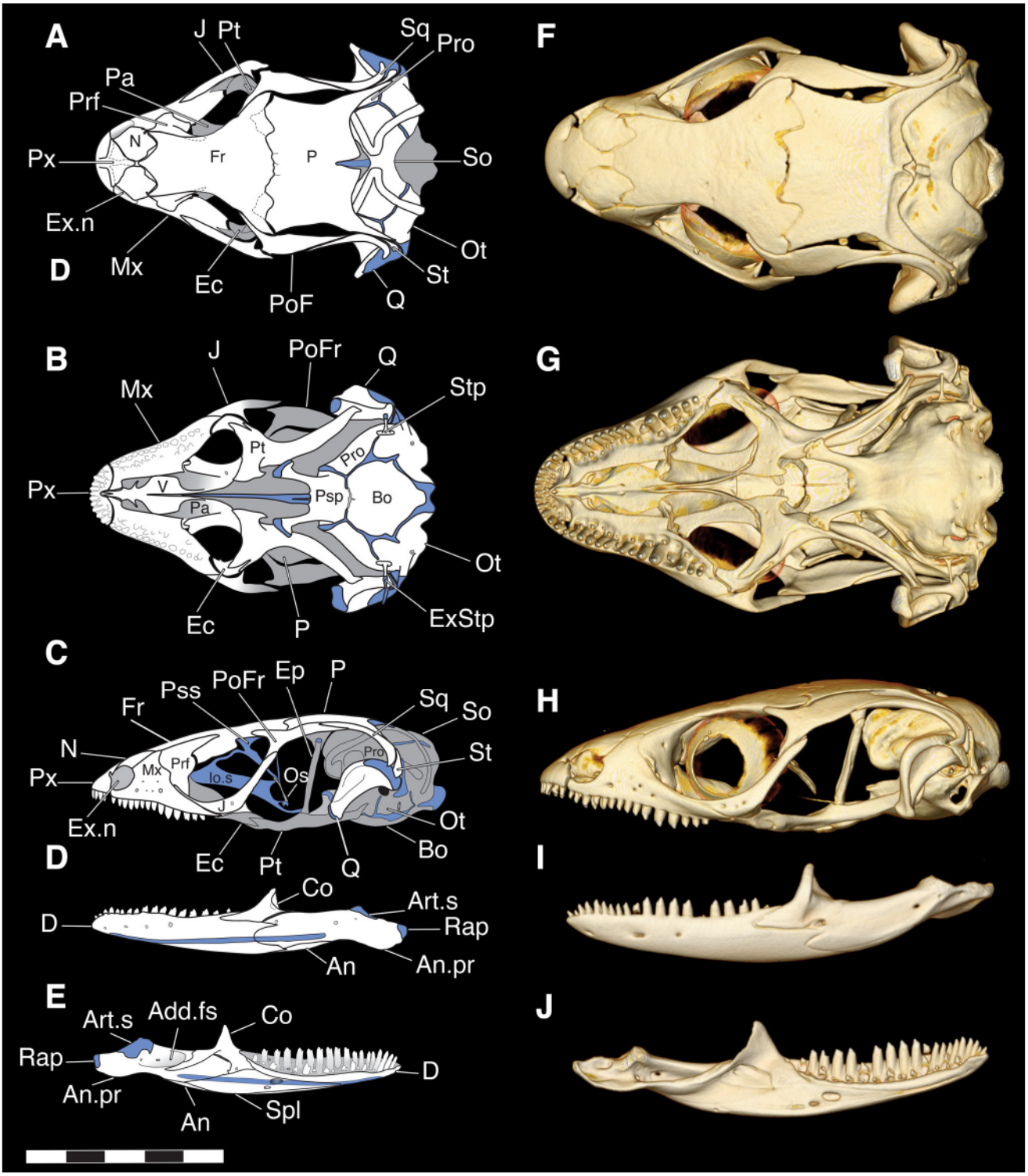

Fig. 2. Skull of *Ptychoglossus vallenssis*. (**A–E**) Drawings of a subadult specimen (CD-UV 2034), the blue parts represent cartilaginous elements, and the white parts are ossified; (**F–J**) CT scans of AMNH119239 (paratype). (A, F) dorsal view of the cranium; (B, G) ventral view of the cranium; (C, H) lateral view of the cranium; (D, I) lateral view of the jaw; (E, J) medial view of the jaw. Abbreviations: Add.fs, Adductor fossa; An, angular; An.pr, angular process; Art.s, articular surface; Bo, basioccipital; Co, coronoid; D, dentary; Ec, ectopterygoid; Ep, epipterygoid; Ex.n, external nares; ExStp, extrastapes; Fr, frontal; J, jugal; Mx, maxilla; N, nasal; P, parietal; Pa, palatine; PoFr, postorbitofrontal; Pro, prootic; Os, orbitosphenoid; Ot, otooccipital; Psp, parabasisphenoid; Pss, planum supraseptalis; lo.s, interorbital septum; Pt, pterygoid; Px, premaxilla; Q, quadrate; Rap, retroarticular process; So, supraoccipital; Spl, splenial; Sq, squamosal; St, supratemporal; Stp, stapes; V, vomer. Scale bar = 5 mm.

in the posterodorsal border of the orbit assumed to be the postorbitofrontal or result of the fusion of postorbital and postfrontal as in *Alopoglossus*; however, these bones remain separated in many gymnophthalmids (Presch, 1980; Evans, 2008), the postorbitofrontal forms part of the supratemporal bar. The supratemporal fenestra is almost closed due to the anterior widening of the posterior process of the postorbitofrontal (Fig. 2A,F). The neurocranium is relatively large, and its highest point is positioned at the same level as the dermatocranium. The posterotemporal fossa is reduced (Fig. 2F). The palate shows the incomplete neochoanate condition (Fig. 2B,G), where the vomer overlaps the dorsal surface of the palatal shelf briefly separating the vomeronasal fenestra from the choana (see Lakjer, 1927; Presch, 1976; Rieppel et al., 2008).

The jaw has a straight tooth row and a curved ventral border, resembling a rocking chair runner. The coronoid process is tall, extending above the jaw profile almost half the height of the jaw immediately below the coronoid. The dentary portion of the jaw is very straight in Alopoglossidae, contrary to other gymnophthalmoideans where the dentary portion is slightly curved. The retroarticular process expands gradually and is oriented on the horizontal plane.

Dermatocranium

Premaxilla. The premaxilla (Fig. 3A,B) bears 11 tooth loci, as in other species in the genus (*P. stenolepis* and *P. bicolor*; Hernández-Jaimes et al., 2012). Tooth implantation is hyperpleurodont according to the degree of walling of the bone (Fig. 3B; Alifanov, 1996). Premaxillary teeth are isodont with conical and rounded crowns; interdental space is about one third of the tooth diameter. Resorption pits are present in the lingual side, and there is one row of replacement teeth buds (Fig. 3B).

The shape of the ascending nasal process is similar to an inverted funnel (Fig. 3A). The shape of the tip varies among the specimens, from square to round. The ascending nasal process has two laminar wings with a dorsomedial facet that establish a lap joint with the nasals. The ascending nasal process forms the anterior edge of external nares, and near the base of the process, it has two lateral indentations that become part of the external nares (Fig. 3A,C,F,H). The medial portion of the ascending nasal process reaches a width almost as wide as the premaxillary dental row. The premaxillary process of the maxilla contacts the palatal shelf of the premaxilla medially. The premaxilla, maxilla, and vomer form the edge of a drop-shaped incisive fenestra (Fig. 2B,G). The palatal shelf of the premaxilla is notched at the midline (Fig. 3B). There are two pairs of foramina that are connected through a canal: the first pair opens on the ventral side, near the base of the ascending nasal process; the second pair opens on the dorsal surface of the palatal process shelf. Similar canals have been identified as small foramina for cutaneous branches of the anterior ethmoidal nerve (Oelrich, 1956), which corresponds to an anterior branch of the ophthalmic division of the trigeminal nerve (Bell et al., 2003).

Maxilla. The maxilla (Fig. 3C–E) bears between 14 and 18 tooth loci, teeth are arranged in a straight row. The maxillary teeth are bicuspid and have one or two rows of replacement teeth buds on the palatal shelf (Fig. 3D). Tooth height is variable, teeth 5–10 being larger than the anterior and posterior ones.

The posterior process of the maxilla tapers posteriorly (Fig. 3E). The dorsal surface of the posterior process has two facets, a lateral facet that supports the suborbital process of the jugal and another medial facet that contacts the maxillary process of the ectopterygoid. The jugal is visible in the lateral view and overlaps with the maxilla, reaching the lacrimal region (Fig. 2A).

The facial process of the maxilla is triangular with smooth borders and projects posterodorsally (Fig. 3C,D). The facial process forms the posterior edge of the external nares (Fig. 2C,H). The base of the facial process is equivalent to one third of the total length of the maxilla. The facial process contacts the nasal dorsally, and in some specimens, it might contact the frontal. The prefrontal facet of the facial process extensively overlaps the prefrontal. The medial surface of the facial process of the maxilla has a medial ridge (Fig. 3D).

The premaxillary anteromedial process of the maxilla is long and triangular in dorsal view (Fig. 3E). The anterior part of the medial edge of the palatal shelf is straight, and in the middle portion, it forms a palatine facet where the palatine articulates. From this point, the palatal shelf tapers posteriorly, and it becomes concave distally (Fig. 3E). In *P. vallensis*, the dorsal surface of the palatal shelf bears the crista tranversalis (Fig. 3E).

There are two rows of foramina (Fig. 3C), five on the supralabial edge, and two more located at the base of the facial process. The supralabial foramina are connected to the superior alveolar canal that opens on the dorsal surface of the palatal shelf (Fig. 3E).

Nasal. The nasals (Fig. 3I,J) are laminar and dorsally convex. Edges are sinusoid, and the lateral border contributes with the dorsal edge of the external nares (Fig. 2C,H). The anterior and posterior processes of the nasal have convergent edges. The posterior border has a little "C" shaped notch on its lateral edge (sometimes there is a foramen instead of a notch). The medial process of nasal is rounded. The posterior and medial processes of the nasal overlap the anterior portion of the frontal. The lateral edge of the nasal is slightly overlapped for the facial process of the maxilla anterodorsally.

Frontal. The frontal posterior edge is twice the width of the anterior edge (Fig. 3F,G). The interorbital constriction is narrower than the anterior end. The anterior margin of the frontal has three pointed processes (Fig. 3F,G). The medial process is longer than the lateral processes and bifurcates distally, indicating the paired origin of the bone. The nasal facets of the frontal are on the dorsal surface between the medial process and the lateral processes. The lateral edge of the frontal contacts the tip of the facial process of the maxilla and the anterodorsal edge of the prefrontal (Fig. 2A,C). The posterior edge of the frontal has a pair of frontoparietal tabs that project slightly (very subtle in subadult specimens) and articulates with the frontal facets of the parietal (Fig. 2A,F).

The parietal processes of the frontal are lateral to the frontoparietal tabs (Fig. 3F,G). The parietal processes project posterolaterally, having parallel edges and rounded tips. On the lateral edge of the parietal

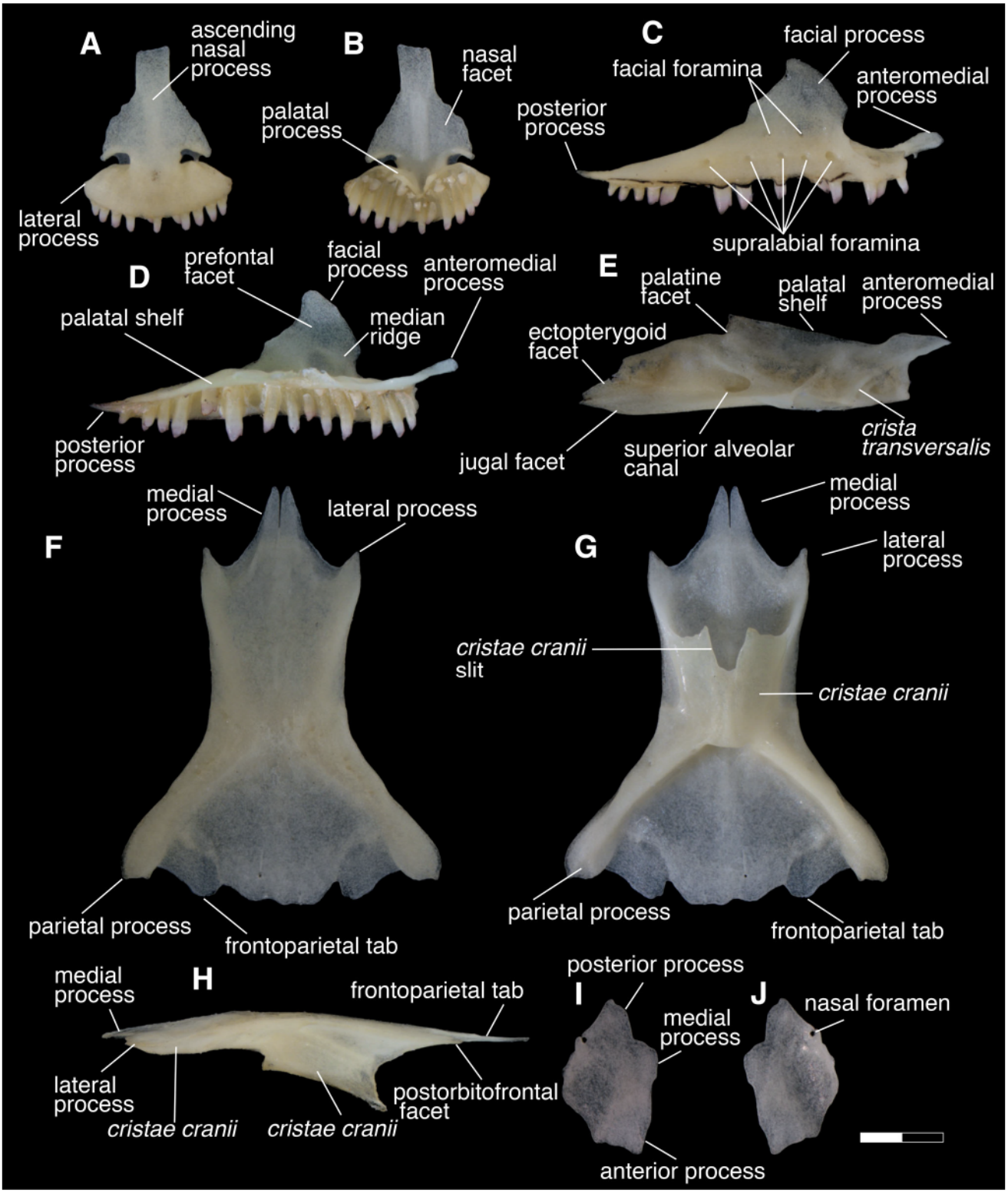

Fig. 3. Individual bones of the skull of the *Ptychoglossus vallensis*. (**A**) Premaxilla anterior view; (**B**) premaxilla posterior view; (**C**) right maxilla lateral view; (**D**) right maxilla medial view; (**E**) right maxilla dorsal view; (**F**) frontal dorsal view; (**G**) frontal ventral view; (**H**) frontal lateral view; (**I**) right nasal dorsal view; (**J**) right nasal ventral view. Scale bar = 1 mm.

processes, there are the facets for the anterior process of the postorbitofrontal.

The ventrolateral surface of the posterior part of the frontal is crossed by the *cristae cranii* as far as the interorbital constriction where it is fused with the other *cristae cranii* forming a tubular structure (Fig. 3G,H). This tubular structure closes the olfactory tract, reaching just behind the base of the medial process of the frontal. Anteromedially, the *crista cranii* has a squared slit, and its anterolateral border contacts the medial surface of the prefrontal (Fig. 3G).

Parietal. The parietal body is rectangular (Fig. 4A–C), and its width is two times its length. The posterolateral processes of the parietal are oriented at a 45-degree angle and taper distally. The length of this process is subequal to the lateral edge of the parietal body. The posterolateral processes contact the supratemporal posterolaterally, the squamosal laterally, and the paroccipital process of the otooccipital (Fig. 2A,C,F,H).

The parietal has a lateral horizontal shelf (Fig. 4A,B). The descending processes are located below this shelf, triangular, laminar, and contact the epipterygoid (Fig. 2C,H; Fig. 4B,C). This process is oriented anteroposteriorly, and it does not reach the posterolateral process. The posterior edge of the parietal shows a posteromedial notch that receives the ascending process of the tectum synoticum (Fig. 2A). The ascending process is cartilaginous in embryos and individuals with immature skeleton (Hernández-Jaimes et al., 2012). The parietal also contacts the anterodorsal surface of the supraoccipital posteriorly. The extent of their contact is variable: in subadults, the posterotemporal fossa is still present whereas it is closed in adults by the increased contact between the parietal and the supraoccipital (Fig. 2A,F).

Prefrontal. The prefrontal (Fig. 4D,E) has three main parts: the facial lamina, the orbitonasal flange, and the dorsal process. The orbitonasal flange of the prefrontal contacts medially the anterolateral surface of the *cristae cranii* of the frontal (Fig. 2C). The ventral edge of the prefrontal lies on the palatal shelf of the maxilla, and in the base of the orbitonasal flange, there is a rounded notch that forms the dorsal border of the lacrimal foramen. The orbitonasal flange is pierced by a tiny foramen. The dorsal process is robust and lies lateral to the frontal for about half of its length. The margins of this process converge gradually toward a rounded tip (Fig. 4D,E).

Postorbitofrontal. The postorbitofrontal (Fig. 4F, G) is a triradiate laminar bone. The posterior process comprises two thirds of the total length of the postorbitofrontal; the anterior part of this process has parallel edges which converge posteriorly forming an acute tip. The posterolateral edge of the posterior process articulates with the squamosal (Fig. 2A,F). The acute anterior process of the postorbitofrontal is triangular, projecting anteromedially, and corresponds to one half of the length of the posterior process. The lateroventral process meets the jugal to form the postorbital bar (Fig. 2C,H).

Squamosal. The squamosal (Fig. 4H) has the typical "hockey stick" shape of squamates (Rieppel, 1994). The anterior half of the squamosal is straight and tapers into an acute tip. The posterior half of the squamosal curves downward to meet the supratemporal medially (Fig. 2A,C). The posterior tip is rounded and inserts into the squamosal foramen of the quadrate. The squamosal forms the posterodorsal corner of the infratemporal fenestra and might contribute to the supratemporal fenestra (Fig. 2A,C,D,H).

Epipterygoid. The epipterygoid (Fig. 4I) is a cylindrical slender bone with slightly expanded epiphysis. The ventral epiphysis inserts into the *fossa columellae* of the pterygoid, whereas the dorsal epiphysis is located on the lateral surface of the descending process of the parietal (Fig. 2C,H). The epiphysis of the epipterygoid remains cartilaginous in subadult specimens (Fig. 2C). In some specimens, there are two foramina in the medial part of this bone, one opening laterally, and one opening medially.

Supratemporal. The supratemporal (Fig. 4J) is a slender bone. Its posterior end contacts three structures: the dorsal surface of the intercalar cartilage; the dorsal surface of the cephalic condyle of the quadrate; and the lateral margin of the paroccipital process. The dorsal end of the supratemporal converges into an acute tip that contacts the squamosal and the posterolateral process of the parietal.

Quadrate. The quadrate (Fig. 4K,L) is a conch-shaped bone, and its lateral surface slightly concave. Lateral to this concavity the tympanic crest extends between the mandibular and cephalic condyles. The posterior part of the quadrate has a central pillar that bears a posterior crest that also extends between the condyles (Fig. 4L). On the medial surface of the quadrate, near the posterior crest, there is a medial crest that extends also between the condyles (Fig. 4K).

The cephalic condyle is located dorsomedially. In subadult specimens, this condyle is cartilaginous (Fig. 2A). In adult specimens, the condyle ossifies and becomes continuous with otooccipital (Fig. 2A,F).

The quadrate has five foramina. Two of them pierce the quadratic conch near the posterior crest. Another foramen is located on the ventral end of the medial crest. These three foramina are communicated via a canal that leads to a fourth foramen, which is located posterodorsal to the mandibular condyle. Lastly, the cephalic condyle has a large foramen, here termed the squamosal foramen (Fig. 2F).

Jugal. The jugal (Fig. 5A–C) is an "L" shaped bone. The suborbital process of the jugal is compressed and extends anteriorly, ending in a bifurcated tip. The postorbital (postorbitofrontal) process of the jugal has convergent edges and a rounded tip. The middle portion of the bone is formed by a curved lamina that is pierced by two or three suborbital foramina (Fig. 5A). The jugal has a medial ectopterygoid process (Fig. 5C). This process is triangular, flat, and contacts the anteroventral portion of the ectopterygoid. The dorsal surface of the ectopterygoid process has a foramen.

Vomer. The vomer (Fig. 5D,E) is a laminar bone. The lateral shelf has a sigmoid border that occupies approximately half the length of the vomer and slightly overlaps the palatal shelf of the maxilla (incomplete neochoanate condition, Fig. 2B,G). The anterior process

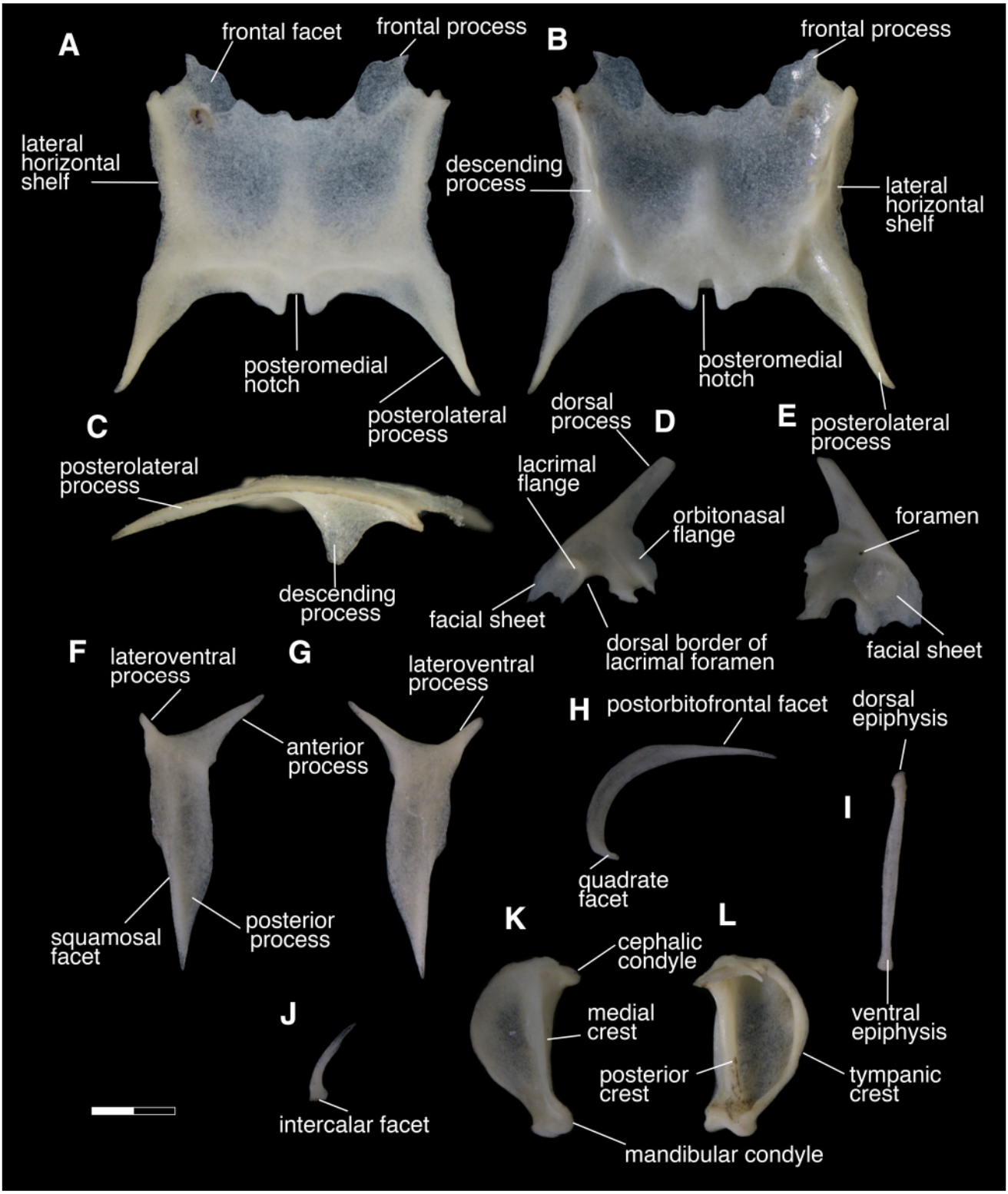

Fig. 4. Individual bones of the skull of the *Ptychoglossus vallensis*. (**A**) Parietal dorsal view; (**B**) parietal ventral view; (**C**) parietal lateral view; (**D**) left prefrontal lateral view; (**E**) left prefrontal medial view; (**F**) left postorbitofrontal dorsal view; (**G**) left postorbitofrontal ventral view; (**H**), right squamosal lateral view; (**I**) right epipterygoid lateral view; (**J**) supratempotal; (**K**) right quadrate medial view; (**L**) right quadrate medial view. Scale bar = 1 mm.

tapers to a point. Between the anterior process and the lateral shelf, the vomer has two processes. The largest is the anterolateral process that overlaps the vomeronasal fenestrae without contacting the palatal shelf of the maxilla. The anterolateral process is triangular with the lacrimal groove on the ventral surface. A second small process is located anterior to the anterolateral process and is half the size of the anterolateral process. The posterior border of this small process forms the anteromedial edge of the vomeronasal fenestra (Fig. 2B,G).

The transversal crest contacts the septomaxilla and lies on the dorsal surface of the lateral shelf of the vomer (Fig. 5D). Posterior to the transversal crest is the vomerine foramen. The medial border of the vomer is crossed from the middle to its anterior part by the dorsal crest, which contacts its counterpart on the other vomer. The slender palatine process of the vomer overlaps ventrally the vomerine process of the palatine.

Palatine. The palatine (Fig. 5F,G) has a ventral concave surface, which forms the choanal groove. The depression becomes increasingly deep anteriorly, leading to the choanal duct where the palatine foramen is located (Fig. 2B,G; Fig. 5F). The palatine is duplicipalatinate (Lakjer, 1927; Rieppel et al., 2008). Anteromedially, the vomerine process becomes compressed. The maxillary process of the palatine is located anterolaterally. This process is wide, slight prominent, with a square tip that articulates with the palatal shelf of the maxilla (Fig. 2B, G). The palatine gradually narrows posteriorly. The pterygoid process has parallel borders and terminates in a pointed tip that overlaps dorsally the palatine process of the pterygoid (Fig. 2B,G). At the base of the pterygoid process, there is a rounded pterygoid facet where the anterior border of the palatine process of the pterygoid contacts.

Pterygoid. The pterygoid (Fig. 5H,I) is flat and "y" shaped bone. The medial margin of the pterygoid palatine process is ax-shaped. This process develops a posterior notch that defines a posteromedial process. The base of this process is pierced by a foramen. Anteriorly, the palatine process has little tubercle. The anterolateral flange of the pterygoid bifurcates in two processes, the anterior ectopterygoid process which is triangular and broad, and near its base, the ectopterygoid spine; these two processes form the joint with the ectopterygoid.

The quadrate process is blade-like and oriented posterolaterally. Its distal tip contacts the medial crest of the quadrate (Fig. 2C,G). The dorsomedial surface of the quadrate process has a shallow groove that extends from the *fossa columellae* to the distal part of the quadrate process (Fig. 5I).

Ectopterygoid. The ectopterygoid (Fig. 5J,K) is a flat bone with a bifurcated anterior flange. The maxillary facet is broad, rounded, and bears the maxillary process. This maxillary process is triangular and acute, overlapping the dorsal surface of the posterior process of the maxilla (Fig. 2A). The borders of the ectopterygoid converge posteriorly into a rounded tip.

Septomaxilla. The septomaxilla (Fig. 5L,M) is dome-shaped, with a medial concavity. The septomaxilla is supported ventrally almost completely by the vomer and has a lateral lamina that rests on the palatal shelf of the maxilla. A crest extends across the dorsal surface of the septomaxilla. The dorsal process of the septomaxilla extends from the dorsal part of the septomaxilla to the medial process of the frontal without contacting it.

Neurocranium

Parabasisphenoid. The parabasisphenoid (Figs. 2B and 6) body is roughly square; from the main body, two long basipterygoid processes project anteriorly, slightly inclined laterally. The basipterygoid processes are flattened near the facet for the pterygoid, and they develop a lap joint with the pterygoid. On the dorsal surface of the basal part of the basipterygoid processes lie the inner carotid foramen. There is a faint parasphenoid rostrum, which is mostly embedded in laminar bone and continued distally by the *trabecula communis*, which remains cartilaginous in adults. Behind the *trabecula communis*, there is an ovoid pituitary fossa. Posterior to the pituitary fossa, there is a low *dorsum sellae* that is pierced by the *abducens* nerve (CN VI) foramen. The *dorsum sellae* is continued into the parabasisphenoid alar process. In subadult individuals, there is a rectangular basicranial fenestra at the suture with basioccipital, which is closed in the adult specimens (Fig. 2B,G).

Prootic. The prootic (Figs. 2 and 6) forms the anterior part of the otic capsule. The anterolateral border of the prootic forms the incisura prootica (Fig. 6E); this structure is a "C-shaped," deep, and rounded notch, which allows the passage of the trigeminal nerve (CN V). The posterior border of the prootic forms the anterior edge of the *fenestra ovalis*, where it fits the rounded footplate of the stapes (Fig. 6B,E).

The prootic bears the anterior semicircular canal, which curves anteriorly and joins the *anterior ampulla*, just dorsal to the *incisura prootica*. Ventral to the anterior semicircular canal is the horizontal semicircular canal that runs anteroposteriorly through the prootic and connects with the horizontal ampulla. The alar process of the prootic is rounded and compressed. The alar process is dorsal to the anterior semicircular canal (Fig. 6E).

The prootic crest crosses the ventrolateral surface of the prootic and runs from the parabasisphenoid joint across the lateral side of the prootic (Fig. 6B). The foramen for the facial nerve (CN VII) is adjacent to the posterior tip of the prootic crest.

Otooccipital. The otooccipital (Figs. 2 and 6) forms the posterolateral portion of the otic capsule. This bone also contributes to the lateral border of the occipital condyle and bounds laterally the foramen magnum (Fig. 6D). The anterior border has a "C" notch that forms the posterior edge of the *fenestra ovalis* (Fig. 6E). The paroccipital process is located posterolaterally to the *fenestra ovalis*. The bulge of the horizontal semicircular canal runs anteroposteriorly on the lateral surface of the otooccipital, and the bulge of the posterior semicircular canal runs posteriorly. The sphenoccipital tubercle is located at the junction of the otooccipital and the basioccipital (Fig. 6B). This tubercle is ventral to the *fenestra ovalis*, between them opens the ellipsoid lateral opening of the recessus scalae tympani (Fig. 6B,E). The second epibranchial contacts the braincase in a small concavity ventral to the paroccipital

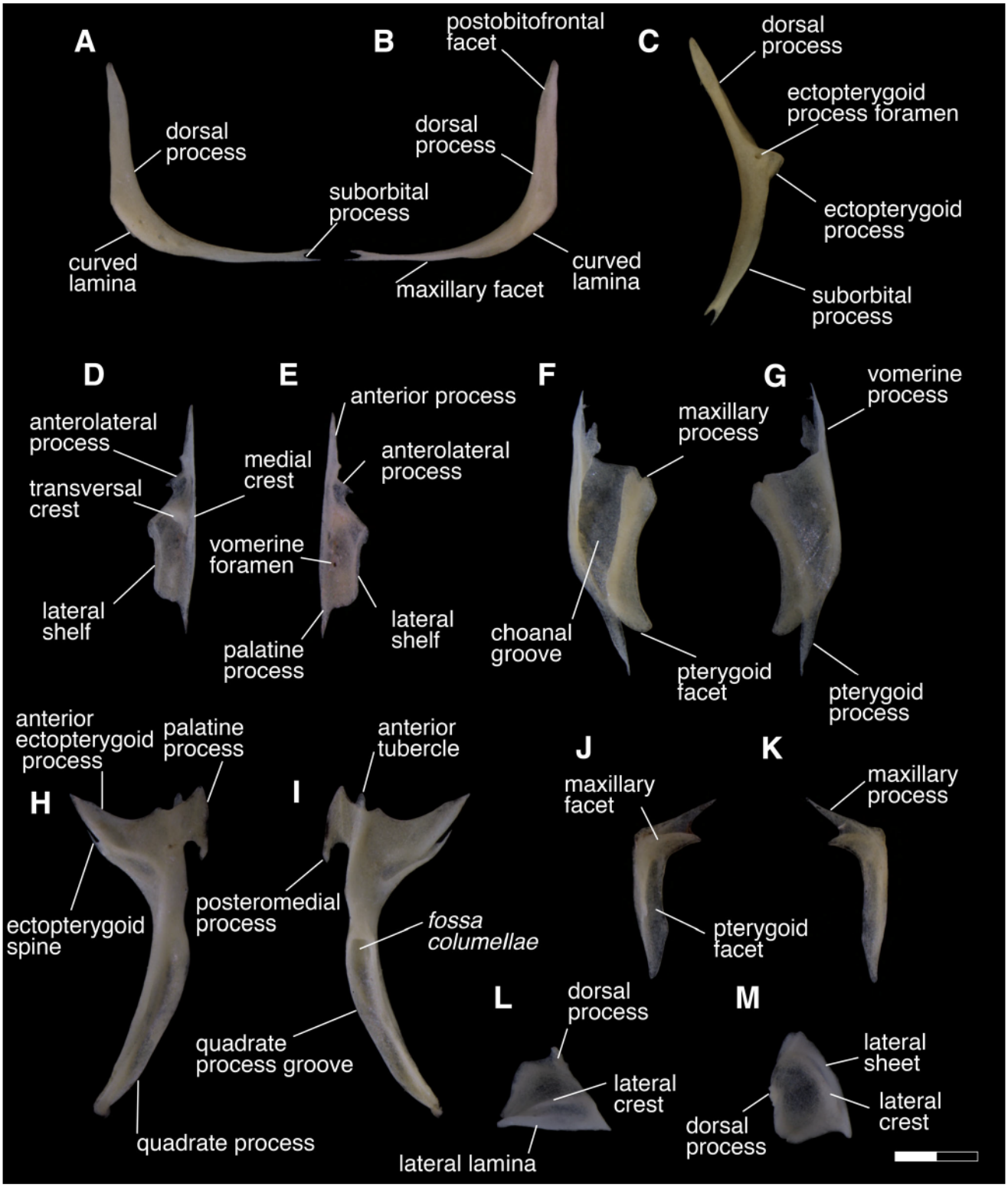

Fig. 5. Individual bones of the skull of the *Ptychoglossus vallensis*. (**A**) Right jugal lateral view; (**B**) right jugal medial view left vomer ventral view; (**C**) right jugal dorsomedial view; (**D**) left vomer dorsal view; (**E**) left vomer ventral view; (**F**) left palatine ventral view; (**G**) left palatine dorsal view; (**H**) right pterygoid ventral view; (**I**) right pterygoid dorsal view; (**J**) left ectopterygoid ventral view; (**K**) left ectopterygoid dorsal view; (**L**) right septomaxilla lateral view; (**M**) right septomaxilla dorsal view. Scale bar = 1 mm.

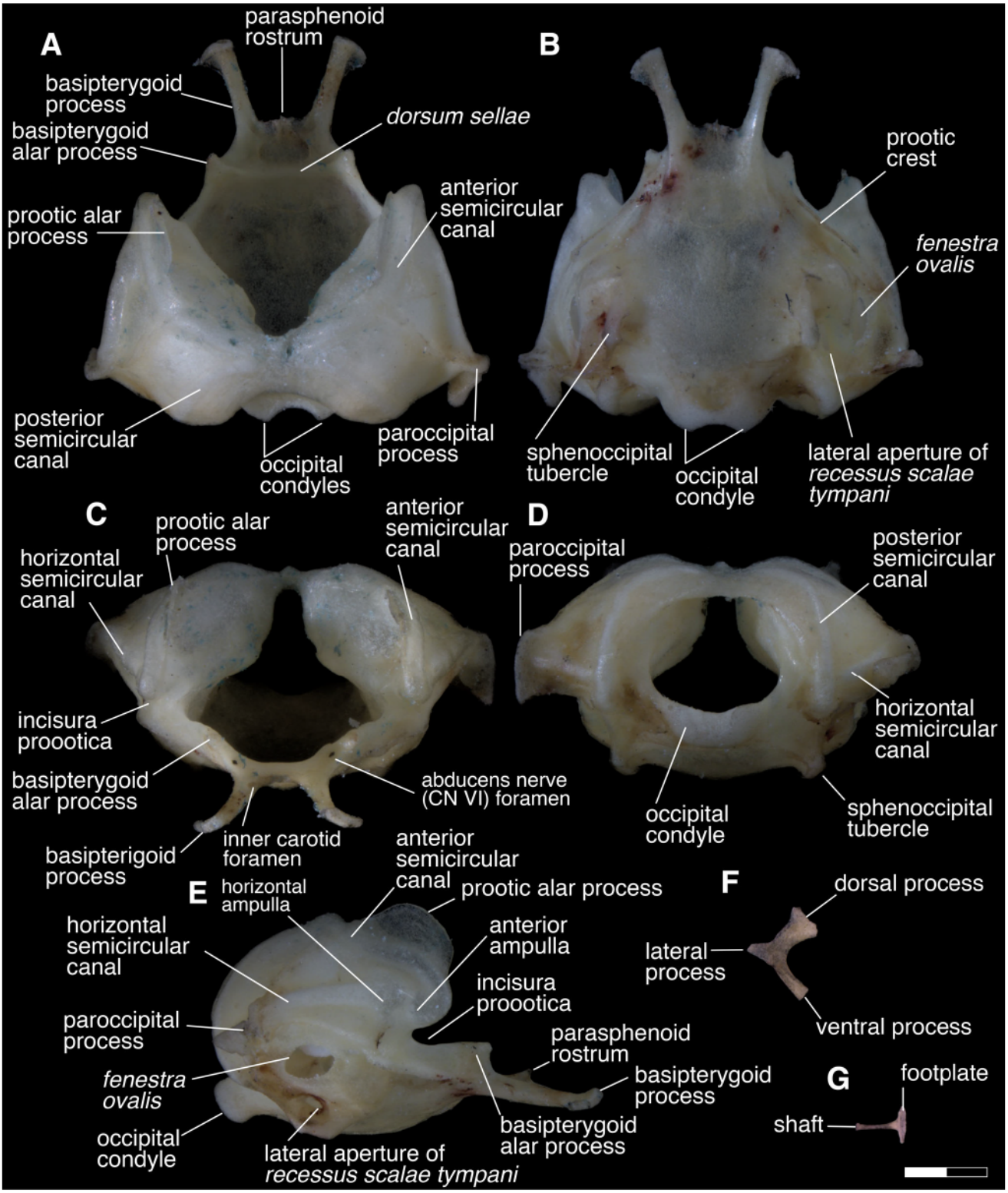

Fig. 6. Braincase of *Ptychoglossus vallensis* in (**A**) dorsal view, (**B**) ventral view, (**C**) anterior view, (**D**) posterior view, and (**E**) lateral view. (**F**) Orbitosphenoid and (**G**) stapes. Scale bar = 1 mm.

process (Fig. 8). Lateral to the occipital condyle, there are two foramina for the hypoglossal nerve (CN XII), and near the lateral edge of the foramen magnum is the foramen for the passage of the vagus nerve (CN X).

Basioccipital. The basioccipital (Figs. 2C and 6B) is a pentagonal-shaped and shield-like bone. The posterior borders converge at a 45-degree angle. The basioccipital forms the ventral portion of the occipital condyle (Fig. 2C).

Supraoccipital. The supraoccipital (Figs. 2A,F and 6A) is hourglass-shaped. The lateral flanges overlap the otic capsules. The expanded lateral flanges are joined by a constricted the medial portion. The ascending process of the *tectum synoticum* is a bar-shaped structure that remains cartilaginous in subadults and becomes calcified in skeletally mature individuals. This process connects the posterior notch of the parietal (Fig. 2A). The posterior border of the medial constriction of the supraoccipital forms the dorsal edge of the foramen magnum (Fig. 6A, D). The anterior and posterior semicircular canals join in the *crus communis* near the midline of the supraoccipital.

Orbitosphenoid. The orbitosphenoid (Fig. 6F) is a compressed bone. It is "L"-shaped with the vertex oriented laterally. It has a wide dorsal process and a slender ventral process, both directed medially. On the vertex of these two processes, there is a small lateral process. Orbitosphenoids are more robust in skeletally mature than in juvenile specimens, where this bone looks very faint.

The orbitosphenoids are joined by chondrocranial structures. The dorsal processes of the orbitosphenoid are joined by the *planum supraseptalis*, which extends toward the posterior part of the *cristae cranii* of the frontal. The ventral processes are united by a dorsal extension of the *septum interorbital.* In turn, the *pila accesoria* is united ventrally to the lateral process of the orbitosphenoid and dorsally to the anterolateral corner of the parietal (Fig. 2C).

Stapes. The stapes (Fig. 6G) is ossified and fits in the *fenestra ovalis* by means of a large and rounded footplate (Fig. 2B). The shaft of the bone is a slender bar. A cartilaginous extrastapes is associated with the stapes. The extrastapes is a tetra-radiated structure, with a basal peduncle that articulates with the stapes. From the distal region, the extrastapes originates three processes: one ventral projected anteriorly; one dorsal projected posteriorly; and the quadrate process projected ventrally.

Mandible

Dentary. This bone (Fig. 7A,B) bears between 20 and 21 teeth loci on the alveolar row (see Table 1). The dental implantation is pleurodont, and the alveolar row is nearly straight. The dorsal borer of the dentary curves posterodorsally. The anterior teeth are procumbent. The dentition is heterodont: the first eight teeth are slender and unicuspid; the remaining teeth are bicuspid, with the posterior crown much larger than the anterior. The absorption pits are on the lingual surface of the teeth. There are one or two rows of replacement teeth buds (Fig. 7B).

The Meckelian groove opens near the mandibular symphysis, and the posterior portion is closed by the splenial bone (Fig. 2J). The symphyseal facet is broad and long, extending posteriorly to the level of the third mandibular tooth (Fig. 7B). The dentary has five mental foramina: the first one is located on the symphyseal region, and the last one is under the midpoint of the dental row (Fig. 7A).

Posteriorly, the dentary contacts the coronoid, surangular, and angular (Fig. 2D,E,I,J). The anteromedial and the labial processes of the coronoid clasp the dentary posterodorsally. The posterodorsal process is triangular and oriented posteriorly. The dentary overlaps the surangular, forming the anteroventral margin of the surangular foramen. The angular process is triangular and is oriented posteroventrally, being almost twice as big as the posterodorsal process. Between the posterodorsal process and the angular processes, there is a wide "U"-shaped posterior notch.

Coronoid. The coronoid (Fig. 7C,D) is a triradiate bone. The anteromedial process is laminar and contacts the dorsal border of the splenial, and its posterior border contacts the surangular (Fig. 2E,J). The surface of the anteromedial process bears one or two foramina near to its posterior border. The posteromedial process is depressed and has an irregular shape that projects posteriorly and establishes a laminar contact with the surangular. The posteromedial process contributes to one third of the adductor fossa edge (Fig. 2E,J).

The coronoid process is tall and has semi-parallel borders, with a rounded eminence. The coronoid and posteromedial processes are continuous by a well-defined medial crest that runs on the medial surface of the coronoid (Fig. 7C,D). The labial process is directed anteriorly. The labial process overlaps the dentary and has margins that gradually converge into a rounded end.

Angular. The angular (Fig. 7J,K) is slender and ends in sharp points. The anterior part overlaps the angular process of the dentary. The angular contacts the compound bone posterodorsally and the ventral border of the splenial medially (Fig. 2D,E,I,J). The posterior foramen for the mylohyoid nerve opens dorsally and has its exit ventrally.

Splenial. The splenial (Fig. 7E,F) is blade-like with sharp anterior and posterior tips. The anterior inferior foramen is oval. The superior mylohyoid foramen is ventral to the anterior inferior foramen and about three times smaller. Posteriorly, the splenial overlaps the compound bone (Fig. 2E,J).

Mandibular compound bone. The size of the compound bone is almost one half of the total length of the jaw (Figs. 2 and 7G,I). In the Gymnophthalmoidea, the compound bone is formed by the post-embryonic fusion of the surangular, prearticular, and articular (Bell et al., 2003; Tarazona et al., 2008).

The surangular portion forms the dorsal wall of the adductor fossa. On the lateral surface of the surangular there are three foramina. Ventral to the contact with the coronoid is the anterior surangular foramen that opens medially where is overlapped by the dentary (Fig. 7G, I). The lateral wall of the abductor fossa is pierced by the posterior surangular foramen and another little foramen located posterior to this last (Fig. 7G, I).

The articular/prearticular portion forms the posteromedial and terminal part of the mandible and contributes to

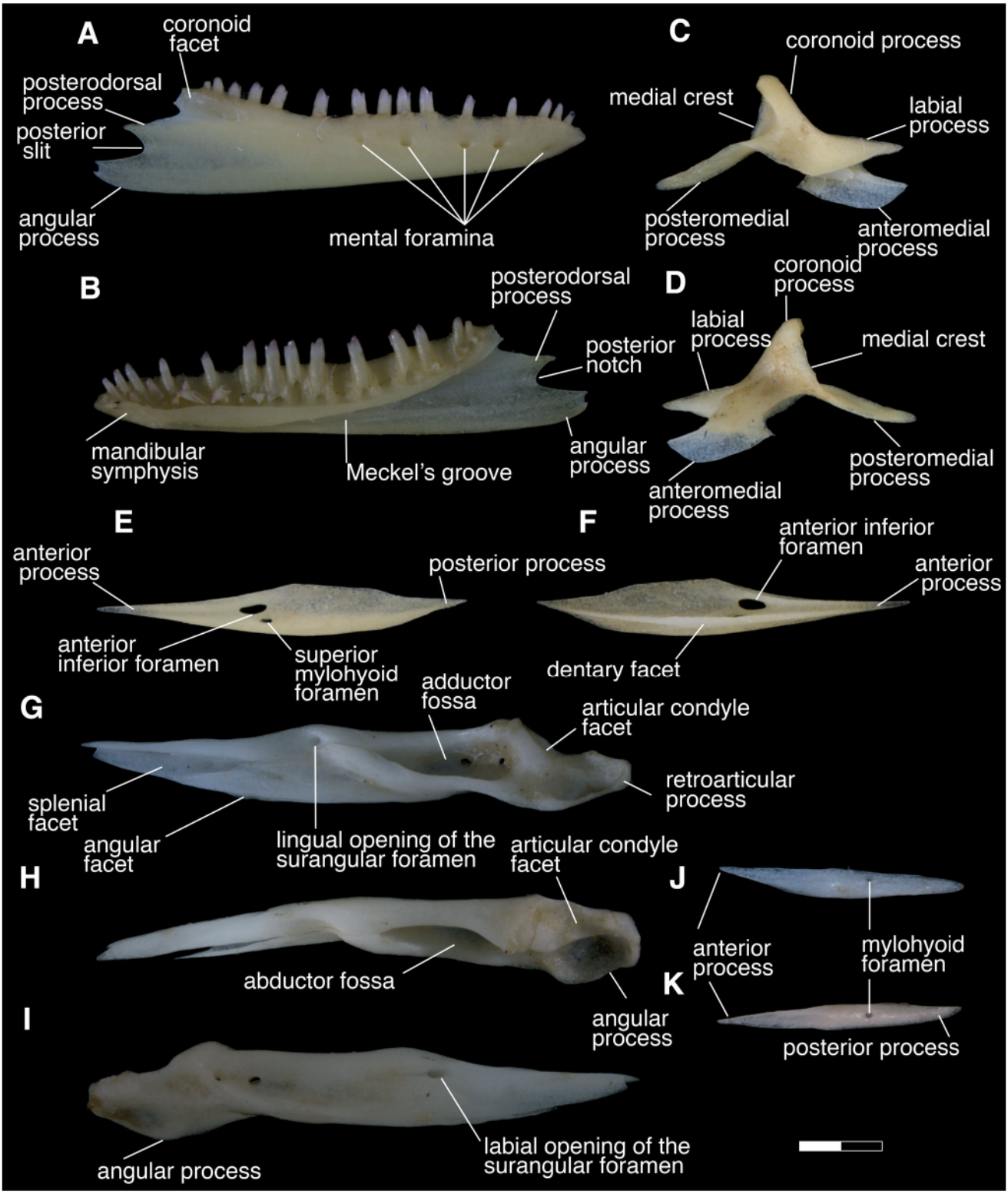

Fig. 7. Individual bones of the jaw of *Ptychoglossus vallensis*. (**A**) Right dentary lateral view; (**B**) right dentary medial view; (**C**) right coronoid medial view; (**D**) right coronoid lateral view; (**E**) left splenial lateral view; (**F**) left splenial medial view; (**G**) right mandibular compound bone medial view; (**H**) right mandibular compound bone dorsal view; (**I**) right mandibular compound bone lateral view; (**J**) left angular dorsal view; (**K**) left angular in ventral view. Scale bar = 1 mm.

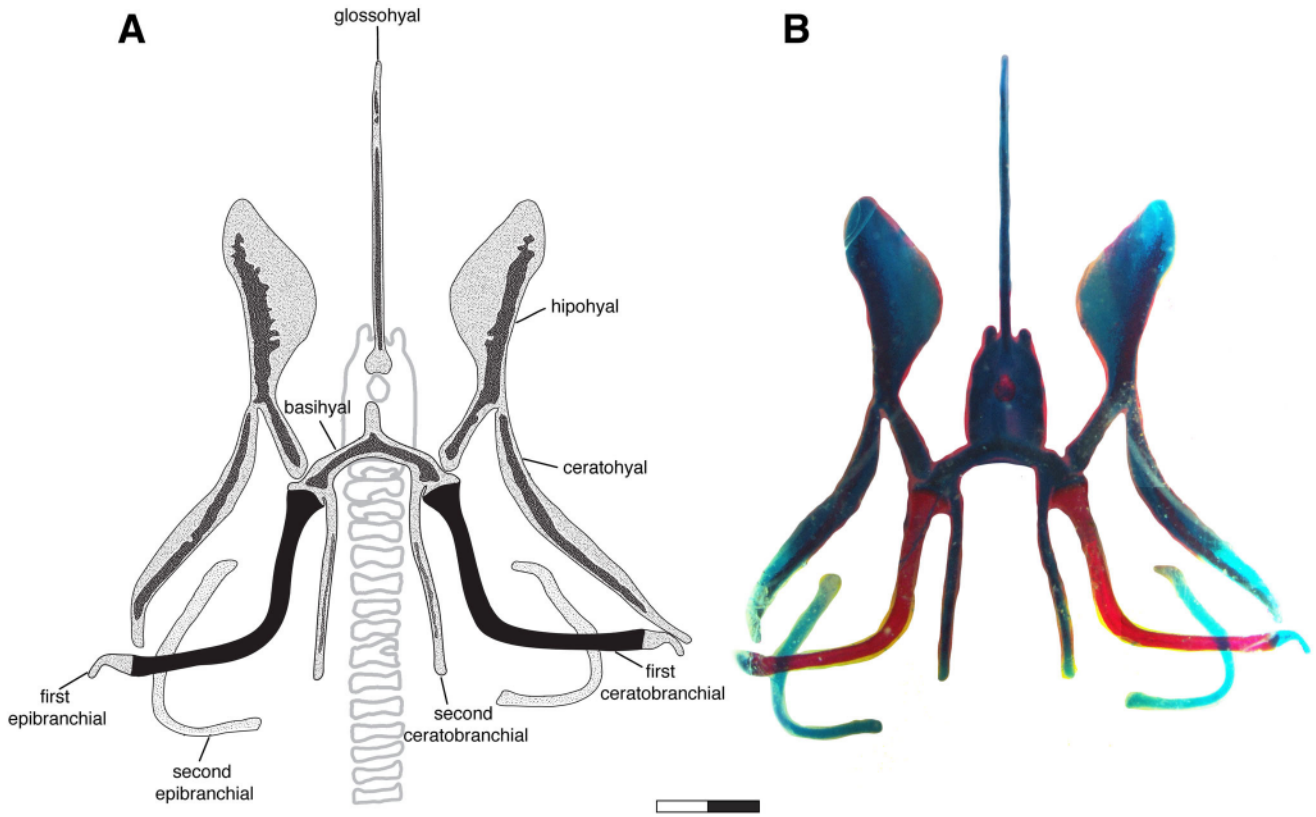

Fig. 8. Hyoid apparatus of *Ptychoglossus vallensis*. (**A**) Draw of the hyoid apparatus, the pointed parts represent cartilaginous elements and the solid dark parts are ossified. (**B**) Photograph of the hyoid apparatus. Scale bar = 1 mm.

the ventral edge of the adductor fossa. The articular condyle facet is located anterior to the retroarticular process. Ventromedial to the articular condyle facet are two small foramina and the foramen for the chorda tympani branch of the facial nerve that opens in the posterior part of the adductor fossa. The posterior portion of the retroarticular process and the facet for the articular condyle of the quadrate are cartilaginous in subadult specimens, becoming ossified in adults. The angular process has a dorsomedially oriented concavity and projects ventromedially (Fig. 7H).

Hyoid apparatus. The basihyal is the central element of the hyoid apparatus (Fig. 8). This structure is triradiate with an anterior process and two posterolateral processes. The anterior process extends up to the level of the laryngeal foramen, with parallel borders and a rounded tip. The glossohyal is long, slender, reaches the level of the last tooth of the dentary anteriorly, and is detached from the basihyal. The posterior part of the glossohyal abruptly widens to form a rounded structure.

Three paired elements are associated with the posterolateral processes of the basihyal. The hipohyal articulates with a slight concavity on the anterior border of the posterolateral process. The hipohyal is directed anterolaterally and reaches the level of the middle part of the glossohyal. The posterior third of the hipohyal has parallel borders, and the anterior two thirds have a curved medial border and a straight lateral border. The ceratohyal is fused to the lateral border of the hipohyal, projecting posteriorly, and gently curved laterally. The anterior and posterior tips of the ceratohyal are narrow, but the middle part is slightly wider.

The first ceratobranchial is the only ossified element in the hyoid apparatus. It is rounded and wide anterior terminus articulates with the posterolateral process of the basihyal. Posteriorly, the first ceratobranchial is uniformly slender and a hollow shaft. The anterior half of the first ceratobranchial is directed posterolateraly, whereas its middle section is curved, forming a 100-degree angle. The cartilaginous first epibranchial articulates with the distal tip of the first ceratobranchial and projects dorsolaterally up to the level of the quadrate and is gradually narrows distally and has a rounded tip.

The last element connected the basihyal is the second ceratobranchial that is narrow with parallel borders. It projects posteriorly up to near the posterior border of the first ceratobranchial. The second epibranchial is embedded in the side of the neck, oriented perpendicularly to the rest of the hyoid apparatus and articulating with the otooccipital dorsally.

DISCUSSION

Osteological Comparisons Within Gymnophthalmoidea

The Gymnophthalmoidea is a diverse group of lizards (429 species, Uetz et al., 2018) whose members exhibit a diversity of habits such as terrestrial-runners (e.g.,

TABLE 1. Revision of the teeth count in Gymnophthalmoidea based on bibliography and analyzed specimens

Subfamily	Species	Premaxilla	Maxilla	Dentary	Data source
Alopoglossidae	*Ptychoglossus bilineatus*	14	20	25–26	Harris, 1994
	Ptychoglossus bicolor	10–12	13–16	19–21	Harris, 1994; Hernández-Jaimes et al., 2012
	Ptychoglossus gorgonae	11	14–15	19–21	Harris, 1994
	Ptychoglossus plicatus	12	23	28	Harris, 1994
	Ptychoglossus vallensis	11	14–18	20–21	CD-UV 2034, 2051; (Harris, 1994)
	Ptychoglossus stenolepis	11	15	19	CD-UV 3603
Gymnophthlamidae	*Alexandresaurus camacan*	12	21	14–15	Rodrigues et al., 2007
	Bachia bicolor	7–9	11–12	13–15	Tarazona et al., 2008
	Calyptommatus nicterus	8–9	6	12	Roscito and Rodrigues, 2010
	Caparaonia itaiquara	11	14	17	Rodrigues et al., 2009
	Cercosaura schreibersii	10–13	15–18	15–20	Lopez and Cabrera, 1995
	Dryadosaura nordesina	11	12–13	14–15	Rodrigues et al., 2005
	Echinosaura palmeri	15	21–23	27	CD-UV 3223
	Euspondylus acutirostris	11	16–17	18–20	Montero et al., 2002
	Herterodactylus imbrincatus	11	18–19	23–24	MacLean, 1974
	Iphisa elegans	13	24	29	Dixon, 1974
	Neusticurus rudis	9	13–17	17–20	Edmund, 1969
	Nothobachia ablephara	7	8	15	Roscito and Rodrigues, 2010
	Potamites ecpleopus	11	14–18	20	MPEG 13092; (Bell et al., 2003)
	Pholidobolus vertebralis	12	16	20	CD-UV 2013, 2014
	Riama laevis	11	15–16	19	CD-UV 3597
	Riama striata	11	14	16–17	CD-UV 1639
	Rondonops biscutatus	13	24	25	Colli et al., 2015
	Scriptosaura catimbau	9	9–10	15	Roscito and Rodrigues, 2010
	Vanzosaura rubricauda	9–11	13–15	19–21	Guerra and Montero, 2009
Teiidae	*Ameiva ameiva*	13	23	29	MPEG 32080
	Cnemidophorus lemniscatus	7	16	22	MPEG 17313
	Crocodilurus amazonicus	8	15	17	MPEG 18486
	Dracaena guianensis	8	11	12	MPEG 18483, 18,485
	Kentropyx calcarata	12	20	25	MPEG 22298
	Salvator duseni	9–11	15–18	17–19	CEPB 647, 1,442
	Salvator merianae	11	14	16	CEPB 10888
	Tupinambis longilineus	12	16	21	MPEG 20502
	Tupinambis quadrilineatus	11	16	19–20	CEPB 3399, MPEG 16817
	Tupinambis teguixin	11	15–17	18–20	MPEG 18484, 18,488

Cnemidophorus, *Tupinambis*), aquatic (e.g., *Dracaena*, *Potamites*), sand swimming (e.g., *Calyptommatus*), and leaf-litter specialists (e.g., some *Bachia*).

One of the traits that is highly variable in the dentition of the Gymnophthalmoidea is the number of teeth loci (Table 1). Fossorial forms have a reduced number of premaxillary and maxillary teeth (e.g., *Bachia*, *Calyptommatus*, *Notobachia*), whereas the largest numbers are present in running forms such as the teiid *Ameiva* and lowland forest dweller species such as the gymnophthalmid *Echinosaura palmeri* and the alopoglossid *Ptychoglossus bilineatus*. Pleurodont is the more generalize teeth implantation type; although, in *Dracaena* and *Salvator*, implantation is subpleurodont, in which a theca is formed in the lingual side of the tooth reinforces the tooth base (Presch, 1974; Zaher and Rieppel, 1999; Montero et al., 2004; Brizuela and Albino, 2009; Pujos et al., 2009; Brizuela and Albino, 2010). The premaxillary teeth are unicuspid in the Alopoglossidae as well as in the Gymnophthalmidae. The maxillary and dentary teeth are bicuspid in general in the Gymnophthalmidae *s.l.* but some species exhibiting a tricuspid condition in the posterior dentary and maxillary teeth (i.e., *Potamites ecpleopus*; Presch, 1980; Bell et al., 2003). All teeth in gymnophthalmid genera *Bachia*, *Calyptommatus*, *Nothobachia*, and *Scriptosaura* exhibit unicuspid teeth curved posteriorly (Tarazona et al., 2008; Roscito and Rodrigues, 2010). In the case of the Teiidae, tooth morphology is highly variable in the premaxilla, maxilla, and dentary (Presch, 1970, 1974).

Major variation in the dermatocranium of gymnophthalmoids is found in the premaxilla, frontal, parietal, prefrontal, postorbital, postfrontal (postorbitofrontal), lacrimal, palatine, and pterygoid. The ascending nasal process of the premaxilla in *P. stenolepis* has a basal constriction similar to that of *P. vallensis*. This character state is also present in the fossorial gymnophthalmines *Calyptommatus nicterus*, *Scriptosaura catimbau*, and *Nothobachia ablephara* (Roscito and Rodrigues, 2010; Fig. 1). In cercosaurines (*Riama*, *Euspondylus*, *Cercosaura*, *Pholidobolus*, and *Echinosaura*), the ascending nasal process has parallel margins that taper distally and lacks the mentioned basal constriction, although this morphology is different in *Potamites* (Fig. 1, see also MacLean, 1974; Lopez and Cabrera, 1995; Montero et al., 2002; Rodrigues et al., 2007; Rodrigues et al., 2009; Tarazona et al., 2008; Gauthier et al., 2012). The Teiidae shows the same widespread condition of cercosaurines (Presch, 1970; Tedesco et al., 1999). Harris (1994) described that in *P. stenolepis* the premaxilla does not contact the frontal, but we found that in some specimens of *P. stenolepis*, the premaxilla briefly contacts the medial process of the frontal bone, separating the nasals. This same condition was found in all specimens of *P. vallensis*. A similar

premaxilla-frontal contact is found in *Alopoglossus* (e.g., *A. buckleyi* (MacLean, 1974), *A. angulatus* (Rodrigues et al., 2007), and *A. altriventris* (Rodrigues et al., 2009)). In teiids, the internasal contact is universal, whereas the nasals usually are separated in gymnophthalmids (Fig. 1).

The frontal has an interorbital constriction that is approximately one third the width of the posterior margin in cercosaurinids, such as *Potamites ecpleopus* (Bell et al., 2003), *Echinosaura palmeri*, and *Riama laevis*. This contrasts with *P. vallensis* where the interorbital constriction is broader, measuring one half the width of the posterior margin of the frontal. The fronto-parietal joint in the Alopoglossidae and the Gymnophthalmidae is a stepped tongue-in-groove joint (*sensu* Jones et al., 2011); the frontoparietal tabs overlap frontal facets on the dorsal surface of the parietal. The size of the frontoparietal tabs is highly variable within these two families, and even in the same genus: in *P. stenolepis*, the frontoparietal tabs are three times larger than in *P. vallensis*. In the Gymnophthalmidae, large frontoparietal tabs are common in fossorial species, perhaps to prevent or reduced the mesokinetic movements during burrowing and to produce a more rigid dermatocranium (MacLean, 1974; Tarazona et al., 2008; Roscito and Rodrigues, 2010).

The parietal is laminar in the Alopoglossidae, the Gymnophthalmidae, and the Teiinae, whereas it is deflected ventrally forming a half tube in the Tupinambinae. A parietal with a square main body is characteristic of the Alopoglossidae; in some gymnophthalmids, the lateral edge of the parietal is concave, increasing the size of the supratemporal fenestra (e.g., *Riama unicolor*, *Potamites ecpleopus*, *Riama laevis*, *Pholidobolus vertebralis*, and *Echinosaura palmeri*). The descending process of the parietal is markedly smaller and does not reach the base of the posterolateral process in *Alopoglossus* and *Ptychoglossus*. In contrast, the descending process of Teiidae and several gymnophthalmids (*P. ecpleopus*, *R. laevis*, *P. vertebralis*, and *E. palmeri*) crosses the parietal anteroposteriorly, including the posterolateral process. In some fossorial gymnophthalmids, such as *Bachia bresslaui*, *B. bicolor,* and *Calyptommatus nicterus*, the descending process of the parietal is hypertrophied covering the infratemporal fenestra and corresponding reduction on the length of the epipterygoid.

The postfrontal and postorbital fusion has been reported in several Squamata clades (Daza and Bauer, 2012; Palci and Caldwell, 2013), including the Alopoglossidae (*Alopoglossus* and *Ptychoglossus*), the Gymnophthalmidae (*Calyptommatus*, *Dryadosaura*, *Anotosaura* and *Colobosauroides*), and the Teiidae (*Ameiva*, *Cnemidophorus*, *Dicrodon*, *Dracaena*, *Kentropyx* and *Teius* (Presch, 1970, MacLean, 1974, Presch, 1980, Rodrigues et al., 2005, Roscito and Rodrigues, 2010, Hernández-Jaimes et al., 2012)). An analysis of the developmental series of *Calyptommatus sinebrachiatus* suggests that the postorbitofrontal is formed from the fusion between a reduced postfrontal and a well-developed postorbital (Roscito and Rodrigues, 2012). *Ptychoglossus bicolor* also exhibited fusion of the postorbital and postfrontal during its ontogenetic development, although the specific contribution of the postorbital and postfrontal was not specified (Hernández-Jaimes et al., 2012). We expect that what is seen in the adults of *P. vallensis* is also result of the fusion of the postorbital and postfrontal. Understanding the developmental origin of the postorbitofrontal in the Alopoglossidae requires a hypothesis of structural homology, especially in relation to the convergence mentioned above in some gymnophthalmids and teiids.

The presence of a lacrimal bone is variable among the Alopoglossidae. This bone is present in *Alopoglossus atriventris*, *A. buckleyi*, *A. festae*, and *P. bicolor* but is absent in *P. festae* and *P. vallensis*. The lacrimal is also present in the gymnophthalmid genera *Anadia*, *Bachia*, *Echinosaura*, *Gymnophthalmus*, *Heterodactylus*, *Iphisa*, *Leposoma*, and *Tretioscincus* (Presch, 1980; Hernández-Jaimes et al., 2012), whereas in the Teiidae, the lacrimal is always present (Presch, 1970).

The prefrontal and the palatine are not in contact in *P. vallensis*, whereas in *Bachia bicolor*, *Riama laevis*, *Echinosaura palmeri*, and all the teiids examined, the orbitonasal flange of the prefrontal contacts the dorsal surface of the palatine. In the Alopoglossidae and the Gymnophthalmidae, the ectopterygoid and the pterygoid develop a stepped joint. This contrasts with the horizontal slot joint in the Teiidae, where the ectopterygoid embraces the pterygoid flange.

The incomplete neochoanate condition of the palate (Lakjer, 1927; Rieppel et al., 2008) is usually present in the Alopoglossidae and the Gymnophthalmidae, but *Bachia bicolor* (Tarazona et al., 2008) and *Calyptommatus nicterus* (Roscito and Rodrigues, 2010) show the paleochoanate condition. Guerra and Montero (2009) described the kinetic neochoanate condition in *Vanzosaura rubricauda*. The paleochoanate condition is the general condition in the Teiidae.

A previous study of squamates reported that gymnophthalmoideans such as *Bachia* and amphisbaenians shared similar ossification sequences in the floor of the anterior braincase (Bellairs and Gans, 1983, see also Tarazona and Ramírez-Pinilla, 2008); this similarity once proposed to be product of parallel evolution, might be a synapomorphy of the Lacertoidea, which is constituted by gymnophthalmoideans, Lacertidae, and Amphisbaenia.

The Alopoglossidae has long and slender basipterygoid processes. In the Teiidae and some gymnophthalmid species such as *Iphisa elegans*, *Gymnophthalmus especiosus*, *Cercosaura schreiberssii*, *Euspondylus acutirostris*, *Potamites ecpleopus*, *Calyptommatus nicterus*, *Nothobachia ablephara*, and *Scriptosaura catimbau*, these processes are short and stout.

In the jaw, the posterodorsal process of the dentary is well developed in the Alopoglossidae and the Teiidae. The Cercosaurinae has species with a marked trend for the reduction of the posterodorsal process (e.g., *Riama unicolor*, *R. laevis*, *R. striata*, *Bachia bicolor*, *Cerosaura schreibersii*, *Echinosaura palmeri*, *Potamites ecpleopus*, and *Pholidobolus montium*). In the Gymnophthalminae, the pattern is similar to that described for the Alopoglossidae and the Teiidae, except for *Nothobachia ablephara*, which has an extra process between the angular and posterodorsal processes (Roscito and Rodrigues, 2010). In the Teiidae, the angular process of the articular/prearticular complex is large and ventrally oriented whereas in the Alopoglossidae and the Gymnophthalmidae is reduced and medially oriented.

Miniaturization

Ruibal (1952) recognized miniaturization as a trend in the Gymnophthalmidae *sensu lato*. He divided current

members of the Gymnophthalmoidea in two major groups: macroteiids (i.e., Teiidae) and microteiids (i.e., Gymnophthalmidae *s.l.*), largely following and early proposal by Boulenger (1885). Reported body size values (Meiri, 2008; snout vent length, SVL) in teiids ranges from 52 to 614 mm ($\bar{x}$ = 132.4 mm), and some species are comparable in ecology and size to some varanids (Pianka et al., 2017). In the Gymnophthalmidae *s.l.*, body size is predominantly small, reported to vary from 24 to 121 mm ($\bar{x}$ = 62.3 mm) in gymnophthalmids and in 33–78 ($\bar{x}$ = 56.8 mm) in alopoglossids (Meiri, 2008). Miniaturization seems to be the ancestral and more widespread condition within the Gymnophthalmoidea, whereas large size is only developed within the Teiidae. Evolution of body size within the Gymnophthalmoidea needs to be further tested using a larger SVL dataset and within a phylogenetic framework that includes more members of the Episquamata.

Miniaturized gymnophthalmoideans express the same limitations other vertebrates, which are constrained the maintain sense organs (eye, inner ear) and central nervous system in minimal functional size (Rieppel, 1984; Hanken and Wake, 1993). In this regard, *P. vallensis*, express all previously identified traits of miniaturized lizards, including a neurocranium that is proportionally bigger than the dermatocranium and allometric increase in size of the otic capsules (Rieppel, 1984).

Body size has a tremendous effect on skull shape (Rieppel, 1984; Hanken and Wake, 1993; Daza et al., 2008). Large gymnophthalmoideans have elongated and somehow narrow snouts (e.g., *Ameiva*, Fig. 1.17, *Tupinambis* (Montero et al., 2004)), whereas within small forms, there are forms with broad skulls (e.g., *Dryadosaura*, Fig. 1.5) or extremely narrow skulls (e.g., *Calyptommatus*, Fig. 1.12; *Vanzosaura*, Fig. 1.8). A study using 2D or 3D morphometrics can shed some light on the evolution of skull shape within this group, especially with the available molecular phylogeny to polarize ancestral states (Goicoechea et al., 2016).

Functional Morphology

The reduction of mobility within the frontoparietal suture seems to be a recurrent process, not only within the Gymnophthalmoidea but extends to the whole clade of Lacertoidea (e.g., Amphisbaenians and related forms such as *Cryptolacerta hassiaca*, Müller et al., 2011). In the Alopoglossidae, the mesokinetic joint tends to be akinetic or to reduced its movement by the development of a stepped tongue in the groove joint (Jones et al., 2011) or frontoparietal tabs (MacLean, 1974; Roscito and Rodrigues, 2010) between the frontal and the parietal. In the Gymnophthalmoidea, the size of the frontoparietal tabs seems to relate to the level of mechanical stress that the skull supports. Semifossorial lizards have frontoparietal tabs with larger area (e.g., *Nothobachia ablephara*, Fig. 1.10) than species that live among the leaf litter (e.g., *Alopoglossus angulatus*), but in both cases, these structures can help to support the stress generated by exploring deep layers of the organic soil (Bolívar-G and Hernández-Morales, 2013). More mobility is present in the Teiidae, where the mesokinetic region has a butt-lap joint (e.g., *Tupinambis quadrilineatus* and *Cnemidophorus lemniscatus*)—these are generally cursorial species and a flexible skull might play an important role in feeding mechanics.

The joints of the bones of the muzzle unit (Frazzetta, 1962) in *P. vallensis* are strengthened by a high level of overlapping among the dorsal nasal process of the premaxilla and the nasals and between the facial process of the maxilla and the facial sheet of the prefrontal. The increase in overlapping surfaces is a structural advantage that maximizes the contact area and minimizes the profile (Daza et al., 2008). This can be important to support the dorsally directed forces that are generated by catching relatively big and hard prey, such as coleopterans, which were commonly found in the stomachs of *P. vallensis* (Jefferson Panche, personal communication).

Finally, closure of the posterotemporal fenestra due to the overlapping of the parietal on the supraoccipital restricts the movement of the neurocranium in relation to

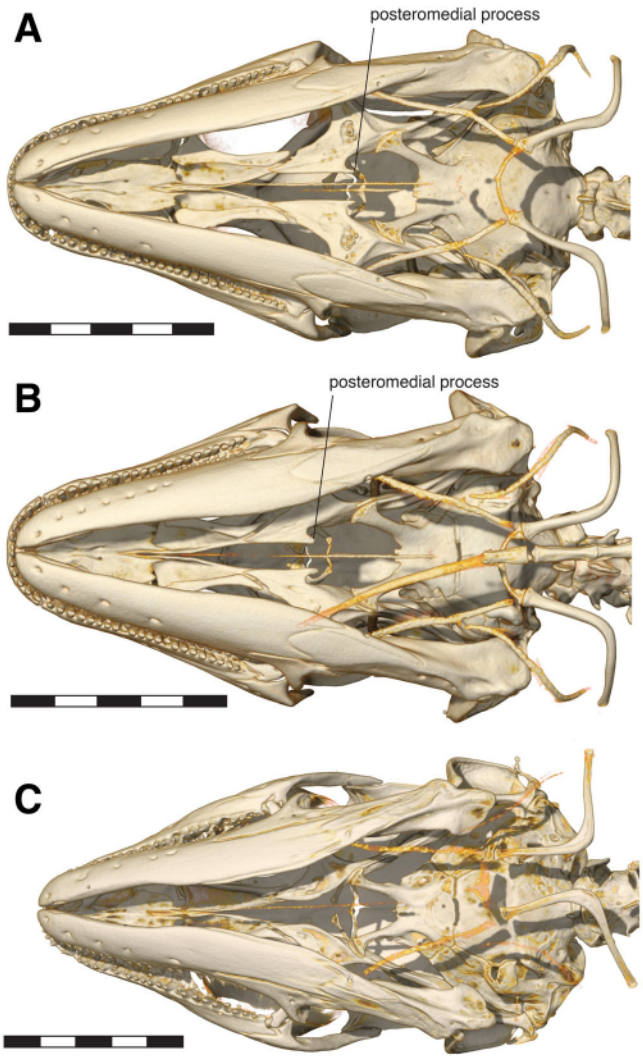

Fig. 9. Ventral view of three gymnophthalmoideans showing the ax-shaped pterygoid in alopoglossideans: (**A**) *Alopoglossus buckleyi* (AMNH113762) and (**B**) *Ptychoglossus plicatus* (AMNH114307), see also Figures 2G and 5H,I for the pterygoid of *Ptychoglossus vallensis*. (**C**) *Loxopholis guianense* (YPM HERR.015357) showing the lack of the posteromedial process. Scale bar = 5 mm.

the dermatocranium or metakinesis (Frazzetta, 1962). Although it is interesting that the joints between the bones of the palate and the pterygoid region are apparently weak, it is reasonable to hypothesize that *P. vallensis* shows an independent streptostyly, with displacement of the quadrates without bending the skull roof at the mesokinetic axis or differently directed turns of the snout and quadrates (Iordansky, 2011). The streptostyly allows the protraction/retraction movement of the maxillary region, which can be largely advantageous for capturing prey.

Morphological Support for Alopoglossidae

The sister taxa relationship between *Alopoglossus* and *Ptychoglossus* have been traditionally supported by few morphological synapomorphies (Boulenger, 1885; Harris, 1994), most of which are convergent with other squamate clades. The dorsal surface of the tongue completely covered for oblique plicae is the only unambiguous synapomorphy described for the Alopoglossidae to date (Boulenger, 1885; Harris, 1994).

The osteological survey of this group allows us to confirm one new putative morphological synapomorphy for the Alopoglossidae: the borders of the palatine process are curved divergently defining a posteromedial process (Fig. 9A,B). In other gymnophthalmoideans, this process has a smooth border with no posteromedial process (Fig. 9C; Bell et al., 2003). This structure hasn't been reported in any other lizard family.

CONCLUSION

In this study, we provided a detailed anatomical description of the skull of *P. vallensis*. Our observations of this taxon, as well as comparisons with other gymnophthalmoideans, resulted in the discovery of a new putative synapomorphy for the Alopoglossidae. It is, however, necessary to expand this detailed anatomical work to other gymnophthalmoidean clades, as well as other squamates. An expanded morphological analysis of the Gymnophthalmoidea might provide better understanding of the phenotypic evolution of these lizards, especially of body size in the Alopoglossidae and the Gymnophthalmidae, and the osteological modifications associated with the miniaturization process.

ACKNOWLEDGMENTS

We thank José Omar Ortiz, Natalia Ferro, and Rodrigo Lozano for their help collecting *P. vallensis* specimens and Gladis Ortiz for allowing field work in her property. We are especially grateful to Julian Mendiví and Juan Felipe Ortega (Universidad del Valle) for their assistance with photographs. We also thank the American Museum of Natural History's Microscopy and Imaging Facility staff (Henry Towbin and Morgan Hill) for help with acquiring and processing CT images. We are extremely grateful to David Blackburn, Edward Stanley, and Daniel J. Paluh (University of Florida) for the training on the processing CT images. We are thankful to Oscar Saenz Manchola who give us important advising on digital illustrations. Aaron Griffing provided extensive corrections on the grammar and contents of the manuscript.

C.H.M. thanks especially to the Smithsonian Institution and Kevin de Queiroz for a Short-Term Grant that allowed him to analyze specimens hosted in several museums in United States. For the loan or access of specimens housed at those institutions, we thank the curators and staff at AMNH (David Kizirian and Lauren Vonnahme), KU (Rafe Brown and Luke Welson), and MPEG (Ana Prudente). C.H.M. was supported by a graduate fellowship from Coordenação de Aperfeiçoamento de Pessoal de Nível Superior (CAPES). P.L.V.P. was supported by grants from Conselho Nacional de Desenvolvimento Científico e Tecnológico (CNPq: grant numbers 313680/2014-0, 400252/2014-7 7). J.D.D received funding from NSF DEB 1657648 and the Department of Biological Sciences at Sam Houston State University.

LITERATURE CITED

Alifanov VR. 1996. Lizards of the families Priscagamidae and Hoplocercidae (Sauria, Iguana): phylogenetic position and new representatives from the late Cretaceous of Mongolia. Paleontol J 30: 100–118.

Bell CJ, Evans SE, Maisano JA. 2003. The skull of the gymnophthalmid lizard *Neusticurus ecpleopus* (Reptilia: Squamata). Zool J Linn Soc 139:283–304.

Bellairs A'A, Gans C. 1983. A reinterpretation of the amphisbaenian orbitosphenoid. Nature 302:243–244.

Bolívar-G W, Hernández-Morales C. 2013. *Ptychoglossus stenolepis Catálogo de Anfibios y Reptiles de Colombia*, Vol. 1. . p 26–30.

Boulenger GA. 1885. *Catalogue of the lizards in the British Museum (Natural History)*, Vol. I–III. 2nd ed. London: British Museum.

Brizuela S, Albino A. 2010. Variaciones dentarias en *Tupinambis merianae* (Squamata: Teiidae). Cuad Herpetol 24:5–16.

Brizuela S, Albino AM. 2009. The dentition of the neotropical lizard genus *Teius* Merrem 1820 (Squamata Teiidae). Trop Zool 22: 183–193.

Castoe T, Doan T, Parkinson C. 2004. Data partitions and complex models in Bayesian analysis: the phylogeny of gymnophthalmid lizards. Syst Biol 53:448–469.

Colli GR, Hoogmoed MS, Cannatella DC, Cassimiro J, Oliveira JG, Ghellere JM, Nunes PMS, Pellegrino K, Salerno P, Marques S de S, et al. 2015. Description and phylogenetic relationships of a new genus and two new species of lizards from Brazilian Amazonia, with nomenclatural comments on the taxonomy of Gymnophthalmidae (Reptilia: Squamata). Zootaxa 4000:401–427.

Conrad JL. 2008. Phylogeny and systematics of Squamata (Reptilia) based on morphology. Bull Am Mus Nat Hist 310:1–182.

Daza JD, Abdala V, Thomas R, Bauer AM. 2008. Skull anatomy of the miniaturized gecko *Sphaerodactylus roosevelti* (Squamata: Gekkota). J Morphol 269:1340–1364.

Daza JD, Bauer AM. 2012. Temporal bones of the Gekkota support molecular relationships within the Pygopodoidea. J Herpetol 46: 381–386.

Dixon JR. 1974. Systematic review of the Microteiid genus *Iphisa*. Herpetologica 30:133–139.

Doan TM, Castoe TA. 2005. Phylogenetic taxonomy of the Cercosaurini (Squamata: Gymnophthalmidae), with new genera for species of *Neusticurus* and *Proctoporus*. Zool J Linn Soc 143:405–416.

Edmund AG. 1969. Dentition. In: Gans C, editor. *Biology of the Reptilia*. New York: Academic Press.

Estes R, de Queiroz K, Gauthier J. 1988. Phylogenetic relationships within Squamata. In: Estes R, Pregill G, editors. *Phylogenetic relationships of the lizard families: essays commemorating Charles L. Camp*. Stanford: Stanford University Press. p 119–281.

Evans SE. 2008. The skull of lizards and tuatara. In: Gans C, Gaunt AS, Adler K, editors. *Biology of the Reptilia, Vol. 20 Morphology H: The skull of lepidosauria*. Ithaca, NY: Society for the Study of Amphibians and Reptiles. p 1–344.

Frazzetta TH. 1962. A functional consideration of cranial kinesis in lizards. J Morphol 111:287–320.

Gauthier JA, Kearney M, Maisano JA, Rieppel O, Behlke ADB. 2012. Assembling the squamate tree of life: perspectives from the phenotype and the fossil record. Bull Peabody Mus Nat Hist 53:3–308.

Goicoechea N, Frost DR, De la Riva I, Pellegrino KCM, Sites J, Rodrigues MT, Padial JM. 2016. Molecular systematics of teioid lizards (Teioidea: Gymnophthalmoidea: Squamata) based on the analysis of 48 loci under tree-alignment and similarity-alignment. Cladistics 32:1–48.

Guerra C, Montero R. 2009. The skull of *Vanzosaura rubricauda* (Squamata: Gymnophthalmidae). Acta Zool 90:359–371.

Hanken J, Wake DB. 1993. Miniaturization of body size: organismal consequences and evolutionary significance. Annu Rev Ecol Evol Syst 24:501–s519.

Harris DM. 1994. Review of the teiid lizard genus *Ptychoglossus*. Herpetol Monogr 8:226–275.

Hernández-Jaimes C, Jerez A, Ramírez-Pinilla MP. 2012. Embryonic development of the skull of the andean lizard *Ptychoglossus bicolor* (Squamata, Gymnophthalmidae). J Anat 221:285–302.

Hildebrand M. 1968. *Anatomical preparations*. Berkeley and Los Angeles, California: University of California Press.

Hoyos JM. 1998. A reappraisal of the phylogeny of lizards of the family Gymnophthalmidae (Sauria, Scincomorpha). Rev Esp Herp 12:27–43.

Iordansky NN. 2011. Cranial kinesis in lizards (Lacertilia): origin, biomechanics, and evolution. Biol Bull 38:868–877.

Jollie MT. 1960. The head skeleton of the lizard. Acta Zool 41:1–64.

Jones MEH, Curtis N, Fagan MJ, Higgins PO, Evans SE. 2011. Hard tissue anatomy of the cranial joints in *Sphenodon* (Rhynchocephalia): sutures, kinesis, and skull mechanics. Palaeontol Electron 14:1–92.

Köhler G, Diethert HH, Veselý M. 2012. A contribution to the knowledge of the lizard genus *Alopoglossus* (Squamata: Gymnophthalmidae). Herpetol Monogr 26:173–188.

Lakjer T. 1927. Studien über die gaumenregion bei sauriern im vergleich mit anamniern und primitiven sauropsiden. Zool Jahrb Abt Anat Ontog Tiere 49:57–356.

Leary S, Underwood W, Anthony R, Cartner S, Corey D, Grandin T, Greenacre C, Gwaltney-Brant SMMA, Meyer R, Miller D, et al. 2013. *AVMA guidelines for the euthanasia of animals*. 2013 ed. Schaumburg: American Veterinary Medical Association.

Lopez AM, Cabrera MR. 1995. Osteología craneal de *Pantodactylus schreibersii schreibersii* (Weigmann, 1834) y su contribución a la discusión de Gymnophthalmidae (Reptilia). Ann Mus Hist Nat Valparaíso 23:53–62.

MacLean RR. 1974. Feeding and locomotor mechanisms of teiid lizards: functional morphology and evolution. Pap Avul Zool 27: 179–213, Museu de Zoologia da Universidade de São Paulo.

Maisano JA. 2001. A survey of state of ossification in neonatal squamates. Herpetol Monogr 15:135–157.

Maisano JA. 2008. A protocol for clearing and double-staining squamate specimens. Herpetol Rev 39:52–54.

Meiri S. 2008. Evolution and ecology of lizard body sizes. Glob Ecol Biogeogr 17:724–734.

Montero R, Abdala V, Moro S, Gallardo G. 2004. Atlas de *Tupinambis rufescens* (squamata: Teiidae). Anatomía externa, osteología y bibliografía. Cuad Herpetol 18:17–32.

Montero R, Moro SA, Abdala V. 2002. Cranial anatomy of *Euspondylus acutirostris* (Squamata: Gymnophthalmidae) and its placement in a modern phylogenetic hypothesis. Russ J Herpetol 9:215–228.

Müller J, Hipsley CA, Head JJ, Kardjilov N, Hilger A, Wuttke M, Reisz RR. 2011. Eocene lizard from Germany reveals amphisbaenian origins. Nature 473:364–367.

Oelrich TM. 1956. The anatomy of the head of *Ctenosaura pectinata* (Iguanidae). Misc Pub Mus Zool Univ Michigan 94:1–122.

Palci A, Caldwell MW. 2013. Primary homologies of the circumorbital bones of snakes. J Morphol 274:973–986.

Pellegrino KCM, Rodrigues MT, Yonenaga-Yassuda Y, Sites JW Jr. 2001. A molecular perspective on the evolution of microteiid lizards (Squamata, Gymnophthalmidae), and a new classification for the family. Biol J Linn Soc 74:315–338.

Peloso PL, Pellegrino KCM, Rodrigues MT, Ávila-Pires TCS. 2011. Description and phylogenetic relationships of a new genus and species of lizard (Squamata, Gymnophthalmidae) from the Amazonian rainforest of northern Brazil. Am Mus Novit 3713:1–24.

Pianka ER, Vitt LJ, Pelegrin N, Fitzgerald DB, Winemiller KO. 2017. Toward a periodic table of Niches, or exploring the lizard Niche hypervolume. Am Nat 190:601–616.

Presch W. 1974. A survey of the dentition of the macroteiid lizards (Teiidae, Lacertilla). Herpetologica 30:345–349.

Presch W. 1976. Secondary palate formation in microteiid lizards (Teiidae: Lacertilia). Bull South Calif Acad Sci 75:281–283.

Presch W. 1980. Evolutionary history of the South American microteiid lizards (Teiidae: Gymnophthalmidae). Copeia 1980:36–56.

Presch W. 1983. The lizard family Teiidae: is it a monophyletic group? Zool J Linn Soc 77:189–197.

Presch WF. 1970. The evolution of macroteiid lizards: an osteological interpretation. Ph.D. Dissertation. Los Angeles, USA: University of Southern California.

Pujos F, Albino AM, Baby P, Guyot JL. 2009. Presence of the extinct lizard *Paradracaena* (Teiidae) in the Middle Miocene of the Peruvian Amazon. J Vert Paleontol 29:594–598.

Pyron RA, Burbrink FT, Wiens JJ. 2013. A phylogeny and revised classification of Squamata, including 4,161 species of lizards and snakes. BMC Evol Biol 13:1–53.

Rieppel O. 1984. Miniaturization of the lizard skull: its functional and evolutionary implications. In: Ferguson MW, editor. *The structure, development and evolution of reptiles*. New York: Symposia of the Zoological Society of London. p 503–520.

Rieppel O. 1994. The Lepidosauromorpha: an overview with special emphasis on the Squamata. In: Fraser NC, Sues H-D, editors. *In the shadow of the dinosaurs: early Mesozoic tetrapods*. New York: Cambridge University Press. p 23–37.

Rieppel O, Gauthier J, Maisano J. 2008. Comparative morphology of the dermal palate in squamate reptiles, with comments on phylogenetic implications. Zool J Linn Soc 152:131–152.

Rodrigues MT, Cassimiro J, Pavan D. 2009. A new genus of microteiid lizard from the Caparaó Mountains, southeastern Brazil, with a discussion of relationships among Gymnophthalminae (Squamata). Am Mus Novit 3673:1–28.

Rodrigues MT, Freire EMX, Pellegrino KCM, Sites JW Jr. 2005. Phylogenetic relationships of a new genus and species of microteiid lizard from the Atlantic forest of north-eastern Brazil (Squamata, Gymnophthalmidae). Zool J Linn Soc 144:543–557.

Rodrigues MT, Machado KC, Dixo M, Verdade VK, Sites JW. 2007. A new genus of microteiid lizard from the Atlantic Forests of state of Bahia, Brazil, with a new generic name for *Colobosaura mentalis*, and a discussion of relationships among the Heterodactylini (Squamata, Gymnophthalmidae). Am Mus Novit 3565:1–27.

Roscito JG, Rodrigues MT. 2010. Comparative cranial osteology of fossorial lizards from the tribe Gymnophthalmini (Squamata, Gymnophthalmidae). J Morphol 271:1352–1365.

Roscito JG, Rodrigues MT. 2012. Skeletal development in the fossorial gymnophthalmids *Calyptommatus sinebrachiatus* and *Nothobachia ablephara*. Zoology (Jena) 115:289–301.

Ruibal R. 1952. Revisionary studies of some South American Teiidae. Bull Mus Comp Zool 106:477–529.

Tarazona OA, Fabrezi M, Ramírez-Pinilla MP. 2008. Cranial morphology of *Bachia bicolor* (Squamata: Gymnophthalmidae) and its postnatal development. Zool J Linn Soc 152:775–792.

Tarazona OA, Ramírez-Pinilla MP. 2008. The unusual orbitosphenoid of the snakelike lizard *Bachia bicolor*. J Anat 213:120–130.

Tedesco ME, Krause L, Alvares BB. 1999. Descripción del sincráneo de *Ameiva ameiva* (Linnaeus) (Squamata, Teiidae). Rev Bras Hematol 16:1025–1044.

Uetz, P, Freed, P. Hošek J. 2018. The reptile database, Available at: http://www.reptile-database.org [Accessed August 2018].

Zaher H, Rieppel O. 1999. Tooth implantation and replacement in Squamates, with special reference to mosasaur lizards and snakes. Am Mus Novit 3271:1–19.